

RESEARCH ARTICLE

10.1002/2017MS001161

# Evaluation of CMAQ Coupled With a State-of-the-Art Mercury Chemical Mechanism (CMAQ-newHg-Br)

Zhuyun Ye<sup>1</sup>, Huiting Mao<sup>1</sup>, Charles T. Driscoll<sup>2</sup>, Yan Wang<sup>3</sup>, Yanxu Zhang<sup>4</sup>, and Lyatt Jaeglé<sup>5</sup>

**Key Points:**

- CMAQ-Hg was modified by implementing a state-of-the-art algorithm depicting Hg reactions and bromine (Br) chemistry (CMAQ-newHg-Br)
- CMAQ-newHg-Br demonstrated improved simulation of seasonal variations in gaseous oxidized mercury (GOM) and particulate bound mercury (PBM)
- Hg wet and dry deposition simulated by CMAQ-newHg-Br showed significantly better agreement with observations and observation-based estimates

<sup>1</sup>Department of Chemistry, State University of New York College of Environmental Science and Forestry, Syracuse, NY, USA, <sup>2</sup>Department of Civil and Environmental Engineering, Syracuse University, Syracuse, NY, USA, <sup>3</sup>School of Environmental Science and Engineering, Shandong University, Jinan, Shandong, China, <sup>4</sup>School of Atmospheric Sciences, Nanjing University, Nanjing, Jiangsu, China, <sup>5</sup>Department of Atmospheric Sciences, University of Washington, Seattle, WA, USA

**Correspondence to:**

H. Mao,  
hmao@esf.edu

**Citation:**

Ye, Z., Mao, H., Driscoll, C. T., Wang, Y., Zhang, Y., & Jaeglé, L. (2018). Evaluation of CMAQ coupled with a state-of-the-art mercury chemical mechanism (CMAQ-newHg-Br). *Journal of Advances in Modeling Earth Systems*, 10. <https://doi.org/10.1002/2017MS001161>

Received 4 SEP 2017

Accepted 12 FEB 2018

Accepted article online 14 FEB 2018

**Abstract** Most regional three-dimensional chemical transport models neglect gaseous elemental mercury (GEM) oxidation by bromine (Br) radicals and Br chemistry. In this study, the Community Multiscale Air Quality model with its default mercury module (CMAQ-Hg) was modified by implementing a state-of-the-art algorithm depicting Hg reactions coupled with Br chemistry (CMAQ-newHg-Br). Using CMAQ-newHg-Br with initial and boundary concentrations (ICs and BCs) from global model output, we conducted simulations for the northeastern United States over March–November 2010. Simulated GEM mixing ratios were predominantly influenced by BCs and hence reflected significant seasonal variation that was captured in the global model output as opposed to a lack of seasonal variation using CMAQ-Hg’s default constant BCs. Observed seasonal percentage changes (i.e., seasonal amplitude [=maximum – minimum] in percentage of the seasonal average) of gaseous oxidized mercury (GOM) and particulate bound mercury (PBM) were 76% and 39%, respectively. CMAQ-newHg-Br significantly improved the simulated seasonal changes in GOM and PBM to 43% and 23%, respectively, from 18% and 16% using CMAQ-Hg. CMAQ-newHg-Br reproduced observed Hg wet deposition with a remarkably low fractional bias (FB; 0.4%) as opposed to a –56% to 19% FB for CMAQ-Hg simulations. Simulated Hg dry deposition using CMAQ-newHg-Br excluding the GEM + OH reaction agreed well with studies using inferential methods and litterfall/throughfall measurements, and the discrepancy varied over 13%–42%. This study demonstrated the promising capability of CMAQ-newHg-Br to reproduce observed concentrations and seasonal variations of GEM, GOM and PBM, and Hg wet and dry deposition fluxes.

## 1. Introduction

Mercury (Hg) is a global pollutant. Its methylated form has neurotoxic health effects for humans and wildlife (Mason et al., 2006; Miller et al., 2007; Rolfhus et al., 2003). A major source of Hg in water bodies, especially those remote from human activities, is atmospheric Hg deposition (Fitzgerald et al., 1998). Atmosphere Hg speciation is operationally defined as gaseous elemental mercury (GEM), gaseous oxidized mercury (GOM), and particulate bound mercury (PBM). GEM is relatively inert comprising about 75% of the global atmospheric Hg pool (Gustin et al., 2015) with lifetime of 0.5–1 year and is considered as the main form of Hg transported over long distances (Driscoll et al., 2013; Mao et al., 2016). With relatively short atmospheric lifetimes ranging from hours to weeks, GOM and PBM can be emitted directly or produced from oxidation of GEM (Cole et al., 2014). GOM and PBM, the total sum of which was denoted as reactive mercury (RM = GOM + PBM), are readily removed from the atmosphere through wet and dry deposition due to their high solubility in water and low vapor pressure. Therefore, chemistry of atmospheric Hg is an extremely important question to address in order to understand the global Hg cycle.

GEM is also of great concern due to its reemission in the form of GEM after the deposition of speciated Hg and reduction in surface environments (e.g., Smith-Downey et al., 2010; Soerensen et al., 2013). To better understand atmospheric Hg cycling, long-term observation networks have been established to quantify Hg ambient concentrations and wet deposition. In the United States, the Mercury Deposition Network (MDN)

© 2018. The Authors.

This is an open access article under the terms of the Creative Commons Attribution-NonCommercial-NoDerivs License, which permits use and distribution in any medium, provided the original work is properly cited, the use is non-commercial and no modifications or adaptations are made.

has biweekly data of total Hg wet deposition since the mid-1990s, and the Atmospheric Mercury Network (AMNet) has monitored Hg concentrations in ambient air since 2009. Challenges remain in characterizing Hg speciation, understanding Hg redox mechanisms, and to quantifying the role of Hg deposition and surface reemission in Hg cycling (Mao et al., 2016; Zhang et al., 2017). Sophisticated atmospheric Hg models are particularly useful tools to fill the knowledge gaps in these important areas.

Over the last decade, several chemical transport models (CTMs) have been modified to simulate atmospheric mercury. With a “one-atmosphere” approach, the Community Multiscale Air Quality model with Hg chemistry included (CMAQ-Hg; Bullock & Brehme, 2002) has been widely utilized in atmospheric Hg deposition studies (Bash et al., 2014; Bullock et al., 2008, 2009; Grant et al., 2014; Lin et al., 2007, 2012; Myers et al., 2013; Pongprueksa et al., 2008; Sunderland et al., 2008; Vijayaraghavan et al., 2007; Zhang et al., 2012a). To accurately simulate Hg wet and dry deposition, it is essential to reproduce the observed atmospheric concentrations of GEM, GOM, and PBM. Currently, annual mean GEM concentrations can be simulated reasonably well with model bias of 5%–62%, but seasonal variations of GEM were not reproduced very well (Baker & Bash, 2012; Bieser et al., 2014; Holloway et al., 2012). Simulated concentrations were predominantly determined by GEM boundary conditions (BCs; Baker & Bash, 2012; Pongprueksa et al., 2008). However, temporal variations (i.e., diurnal to annual cycles) in GEM were poorly depicted by CMAQ (Baker & Bash, 2012; Gbor et al., 2006, 2007; Lin & Tao, 2003; Wen et al., 2011). Modeled GOM and PBM concentrations using CMAQ-Hg generally showed pronounced biases compared with observations (Baker & Bash, 2012; Bieser et al., 2014; Holloway et al., 2012; Ryaboshapko et al., 2007; Sillman et al., 2007; Zhang et al., 2012a). Sillman et al. (2007) compared CMAQ-Hg simulations with aircraft measurements over the Eastern U.S. for a 12 day period in June 2000 and found more than a factor of two overestimation in GOM concentrations near the Earth surface and a ~35% underestimation aloft. In Baker and Bash (2012), simulated GOM and PBM were a factor of 2–5 higher than observations year round for the continental U.S. Similarly, GOM and PBM were overestimated by a factor of 2–10 for the Great Lakes region (Holloway et al., 2012; Zhang et al., 2012a), and overestimated by 15–257% and 82–380%, respectively, over Central and Northern Europe (Ryaboshapko et al., 2007). In East Asia, surface GOM and PBM concentrations were overestimated by 80–180% in most regions (Lin et al., 2010). Other regional and global Hg models have also found considerable overprediction of GOM and PBM compared with observations (Amos et al., 2012; Ryaboshapko et al., 2007; Seigneur et al., 2004; Selin et al., 2007; Zhang et al., 2012a).

Recent studies (Gustin et al., 2015, and references therein) suggested that GOM observations were underestimated, while the magnitude and direction of the PBM bias was uncertain depending on the measurement setup and environment. Moreover, there are no standard calibrations of these measurements (especially for PBM) yet. Apart from these potential measurement biases, several hypotheses have been formulated to explain the overestimation of reactive Hg species, including uncertainties in anthropogenic emission speciation, underestimated dry deposition velocities, overestimated gas-phase GEM oxidation kinetics, and missing important reduction processes or the influence of boundary inflow (Bieser et al., 2014; Kos et al., 2013; Zhang et al., 2012a). Despite highly uncertain simulations of GOM and PBM, modeled Hg wet deposition simulations have shown surprisingly good agreement with measurements (e.g., 21% fractional bias; Holloway et al., 2012). Since GOM and PBM dominate Hg wet deposition, this reasonable agreement is likely due to compensating errors in multiple simulated parameters which control wet deposition flux (Baker & Bash, 2012; Bieser et al., 2014; Holloway et al., 2012; Zhang et al., 2012a).

As suggested in Lin et al. (2006), GEM oxidation mechanisms are poorly understood and constrained in CMAQ-Hg. Ozone ( $O_3$ ), hydroxyl radical (OH), atomic bromine (Br), bromine monoxide (BrO), hydrogen peroxide ( $H_2O_2$ ), and atomic chlorine (Cl) have all been suggested as possible oxidants of GEM in the atmosphere by theoretical and experimental studies (Horowitz et al., 2017; Subir et al., 2011). In addition to being key process in Arctic mercury depletion events (Holmes et al., 2006; Mao et al., 2010), the Br-induced GEM oxidation pathway is also thought to be significant in midlatitudes as shown by recent mercury modeling and observational studies (Gencarelli et al., 2015; Gratz et al., 2015; Holmes et al., 2009, 2010; Obrist et al., 2011; Shah et al., 2016; Ye et al., 2016). Atmospheric Br chemistry, however, is not depicted in CMAQ-Hg, including Br-initiated Hg oxidation. Sillman et al. (2007) attempted to employ halogen reactions in CMAQ-Hg, but did not draw conclusions on the effects of halogen chemistry in model performance. The very limited halogen reactions and kinetics used in CMAQ-Hg are outdated with respect to the reactions proposed in Dibble et al. (2012). Furthermore, regional model initial conditions (ICs) and BCs are thought to have

significant impacts on Hg simulations, contributing up to 99% of total Hg deposition and about 81% of total atmospheric Hg concentrations (=GEM + GOM + PBM; Baker & Bash, 2012; Holloway et al., 2012; Pongprueksa et al., 2008). Recent modeling studies have used global model output or nested simulations to provide ICs and BCs rather than using constant values for all cells as default ICs and BCs in CMAQ-Hg (Baker & Bash, 2012; Bieser et al., 2014; Lin et al., 2010, 2012; Lu et al., 2014; Myers et al., 2013; Zhu et al., 2015).

To improve the performance of CMAQ-Hg in atmospheric Hg simulations, a state-of-the-art Hg and halogen chemical mechanism (Ye et al., 2016) was implemented in CMAQ, with atmospheric BrO concentrations constrained using an observed BrO profile. Initial and boundary conditions were provided with monthly averaged global model output. Four model configuration cases were conducted for the period of March–November 2010 over the northeastern U.S. Simulated Hg ambient concentrations as well as Hg wet and dry deposition were compared with observations. Intercomparison between the four cases allowed us to investigate the importance of different chemical processes, emissions, and BCs. Based on our findings, research needs for future mercury studies are recommended.

## 2. Methods

### 2.1. Model Description and Application

CMAQ-Hg was set up in a Lambert Conformal domain (Figure 1) over the northeastern United States with a spatial resolution of 12 km × 12 km and 35 vertical layers based on sigma pressure levels. Simulations were run for the period of March–November 2010 with a spin-up of 15 days at the end of February 2010. The year 2010 was chosen for study because of the availability of meteorological input, which was provided by the Atmospheric Model Application and Analysis Branch, Computational Exposure Division, NERL, ORD, U.S. EPA. All CMAQ-Hg simulations were conducted in Extreme Science and Engineering Discovery Environment (XSEDE; Towns et al., 2014).

CMAQ version 5.0.2 was used for this study. It was compiled with the multipollutant version of Carbon Bond 2005 (CB05) photochemical mechanism, which includes toluene and chlorine reactions (Sarwar et al., 2008; Tanaka et al., 2003) with an online photolysis and the multipollutant AERO6 aerosol module (Whitten et al., 2010; Yarwood et al., 2005). The cloud module is comprised of three interactive processes: gas-liquid partitioning based on Henry's equilibrium constants; aqueous chemistry of GEM and Hg<sup>2+</sup>; and heterogeneous sorption of aqueous Hg<sup>2+</sup> to suspended elemental carbon aerosols (ECA) forming PBM (Pleuel & Munthe, 1995). As other aerosol species simulated in CMAQ, PBM was classified into three modes: the Aitken, accumulation, and coarse mode. The Aitken and accumulation mode represent PM<sub>2.5</sub> (particulate matter of diameter equal to or less than 2.5 μm). Photolytic reduction of organic Hg<sup>2+</sup> complexes with dicarboxylic acids (Si & Ariya, 2008) is included in the aqueous chemistry as introduced in Bash et al. (2014). The cloud-water concentration and precipitation rate are used to determine wet deposition of mercury species.

The default CMAQ-Hg includes five gas-phase reactions for the oxidation of GEM by O<sub>3</sub>, OH, H<sub>2</sub>O<sub>2</sub>, Cl<sub>2</sub>, and Cl (Baker & Bash, 2012). The products from these GEM oxidation reactions are allocated to 50% GOM and 50% PBM (Bullock & Brehme, 2002). Here we implemented new detailed mechanisms of Hg and Br chemistry (Ye et al., 2016) in CMAQ-Hg, with all other components remaining unchanged. This modified model is denoted as CMAQ-newHg-Br.

CMAQ-Hg and CMAQ-newHg-Br were driven by meteorological fields simulated using the Weather Research and Forecast (WRF) model (version 3.4; Michalakes et al., 2004; Skamarock et al., 2008). The WRF output was processed using the Meteorology-Chemistry Interface Processor (MCIP version 4.2; Byun & Ching, 1999). In MCIP processing, dry deposition of GOM and PBM are calculated using the M3DRY deposition scheme (Pleim & Byun, 2004). A bidirectional flux scheme implementation by Bash (2010) is used to estimate the GEM exchange between the atmosphere and other environmental compartments. The 2010 anthropogenic emissions were provided by the EPA National Emission Inventory (NEI) 2011 (<https://www.epa.gov/air-emissions-inventories/national-emissions-inventory-nei>). The speciation of

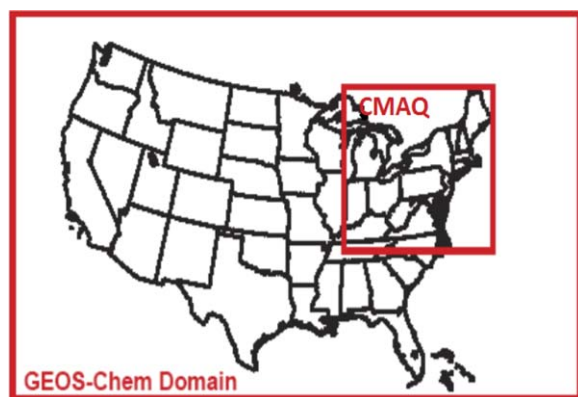


**Figure 1.** The CMAQ model domain and GEOS-Chem model domain for initial and boundary conditions.

**Table 1**  
CMAQ-Hg Case Configurations

Case	Gas-phase Hg chemistry	Br reactions	Hg <sup>0</sup> + O <sub>3</sub> /OH products	IC/BC
DEF	CMAQ-Hg: 4 reactions	No		Profile
DEF_GS	CMAQ-Hg: 4 reactions	No	50% GOM, 50% PBM	GEOS-Chem output
NEW	CMAQ-newHg_Br: 20 reactions	Yes	Dry deposited to the surface	GEOS-Chem output
NEW_noOH	CMAQ-newHg_Br: 19 reactions (without Hg + OH reaction)	Yes	in the first layer, produced as PBM in upper layers	GEOS-Chem output

Hg emissions was referenced in the 2005 version 4.1 platform (<https://www.epa.gov/air-emissions-modeling/2005-version-41-platform>) based on 2005 NEI version 2, and was processed by the Sparse Matrix Operator Kernel Emissions (SMOKE) model (Houyoux et al., 2000).

### 2.1.1. Gas-Phase Hg and Br Chemistry

As aforementioned, the default CMAQ mercury chemical mechanism includes five gas-phase GEM oxidation reactions involving O<sub>3</sub>, Cl, Cl<sub>2</sub>, OH, and H<sub>2</sub>O<sub>2</sub> (Baker & Bash, 2012). Bromine reactions were not included (Lin et al., 2006), and the importance of OH oxidation may be overestimated (Calvert & Lindberg, 2005). Our modified CMAQ-newHg-Br model was employed with detailed, up-to-date Hg (Table A1) and Br chemistry mechanisms (Ye et al. 2016). The new Hg chemical mechanism has 20 (or 19 excluding GEM oxidation by OH) gas-phase Hg reactions which include O<sub>3</sub>, OH, Br, BrO, Cl, Cl<sub>2</sub>, and H<sub>2</sub>O<sub>2</sub> as atmospheric GEM oxidants, as well as reactions of HgBr and HgCl with OH, HO<sub>2</sub>, NO<sub>2</sub>, ClO, BrO to form more stable GOM species (see references in Table A1).

The rate coefficient and the possible pathway of GEM + OH is uncertain (Subir et al., 2011). Although the rate coefficient of this reaction was determined using relative rate experiments (Pal & Ariya, 2004; Sommar et al., 2001), results from theoretical studies (Goodsite et al., 2004; Tossell, 2003) suggest that the reaction is unlikely to occur based on the binding energy calculations of possible products. Moreover, experimental results could be interfered by other compounds such as NO<sub>2</sub> (Calvert & Lindberg, 2005). Two simulations, denoted as NEW and NEW\_noOH (Table 1), were conducted with and without GEM + OH, respectively, to examine the importance of OH in gas-phase GEM oxidation.

The products from GEM + O<sub>3</sub> and GEM + OH reactions were assumed to be 50% of GOM and 50% PBM in the default CMAQ-Hg. Experimental studies suggest that the products of these two reactions could adsorb to the wall of the reaction chamber, forming clusters and aerosols (Jones et al., 2016; Subir et al., 2011 and references therein). Therefore, in NEW\_noOH and NEW the products from these two reactions were assumed to directly deposit to the Earth's surface in the model layer at the surface-atmosphere interface and to form PBM on the surface of aerosols in the upper model layers. All other oxidation reactions assumed 100% gas phase.

There are no Br sources or reactions in the default CMAQ-Hg model. Since Br chemistry is a key component in Hg chemistry, important loss and production reactions of Br (Table A2; Ye et al., 2016) were included in CMAQ-newHg-Br. Considering the complexity and limited understanding of sources of atmospheric Br species (e.g., Chen et al., 2017), an observed BrO vertical profile was used to constrain the Br species. This BrO vertical profile was averaged from all "Tropical Ocean Troposphere Exchange of Reactive halogens and Oxygenated hydrocarbons" (TORERO) research flights data within tropical latitudes over the Eastern Pacific Ocean (Volkamer et al., 2015). Consistent with other measurements (Coburn et al., 2016; Gómez Martín et al., 2013; Wang et al., 2015) conducted over the tropical and midlatitude oceans, BrO mixing ratios are very low (<0.5 pptv) in the marine boundary layer (MBL), probably as low as over land where halogen sources are scarce. Surface BrO concentrations used as constraints in our study was about 0.2 pptv, which agreed very well with those represented in a halogen modeling study by Schmidt et al. (2016) for the North-eastern U.S. A very similar vertical distribution was also derived from TORERO and from Schmidt et al. (2016). Therefore, it seems reasonable to apply this profile for the entire domain, over both land and oceans.

### 2.1.2. Boundary and Initial Conditions

To investigate the relative importance of ICs and BCs, two CMAQ-Hg simulations, denoted as DEF and DEF\_GS (Table 1), were conducted using the default CMAQ-Hg but different ICs and BCs. The DEF case used

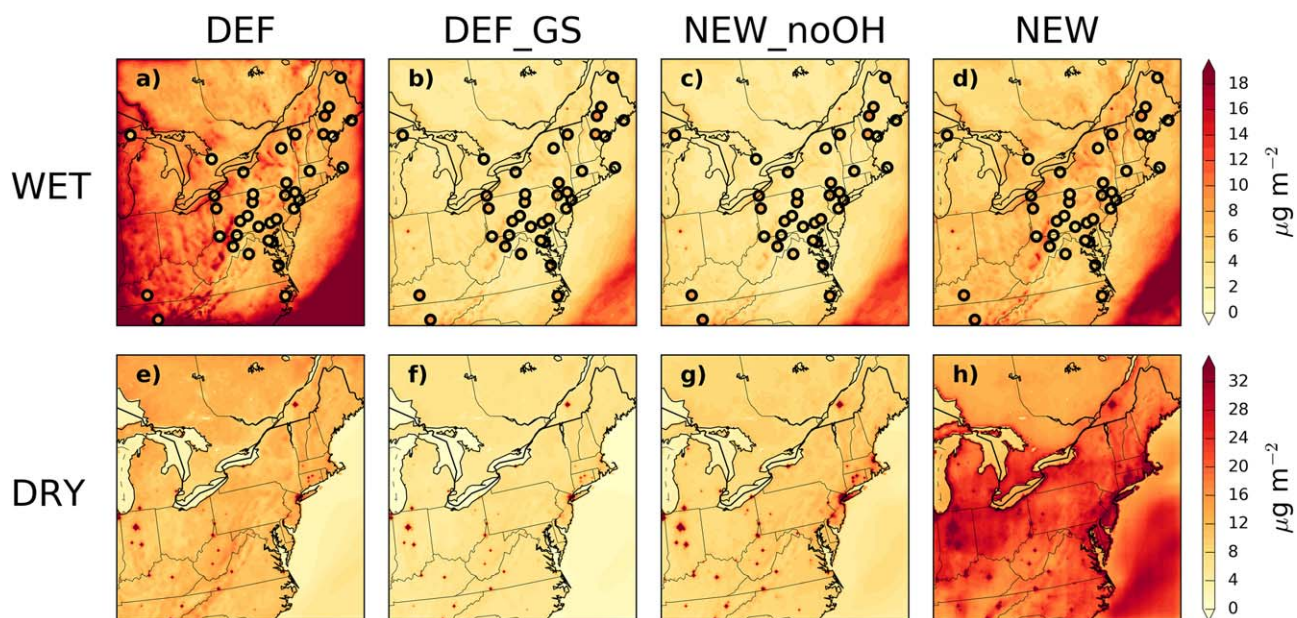


**Figure 2.** Locations of MDN sites (blue solid dots) and ambient speciated Hg monitors (red circle) in the model domain.

the default uniform ICs and time-independent BCs in CMAQ-Hg. Default ICs and BCs for CMAQ-Hg were constant mixing ratios of 178 ppqv for GEM, 2 ppqv for GOM, and 10.8  $\mu\text{g m}^{-3}$  for PBM in time and space over the domain, with only vertical variation. The monthly averaged concentrations for ICs and BCs were provided by a three-dimensional global atmospheric chemistry model GEOS-Chem (version v9-01-02; Zhang et al., 2012c). This GEOS-Chem simulation covered the entire United States continent with a horizontal resolution of  $0.5^\circ \times 0.6667^\circ$  (Figure 1). Detailed information on the configuration of GEOS-Chem can be found in Zhang and Jaeglé (2013) and Zhang et al. (2012c). GEOS-Chem output was also used for ICs and BCs in the NEW and NEW\_noOH cases (Table 1).

### 2.2. Model Evaluation and Data

Simulated ambient concentrations of Hg species were evaluated using March–November 2010 observational data of GEM, GOM, and PBM from Atmospheric Mercury Network (AMNet; <http://nadp.sws.uiuc.edu/amn/>) and the University of New Hampshire (UNH) AIRMAP program (<http://www.eos.unh.edu/observatories/data.shtml>; Figure 2 and Table 2). Note that the Appledore Island (AI) site from AIRMAP and the WV99 site from AMNet did not measure PBM during the study period. Concentrations of atmospheric Hg species were measured at these locations using Tekran speciation units models 2537a/1130/1135, with detection limits of 0.01  $\text{ng m}^{-3}$ , 1.0  $\text{pg m}^{-3}$ , and 1.0  $\text{pg m}^{-3}$  for GEM, GOM, and PBM, respectively (Gay et al., 2013;

**Table 2**  
Atmospheric Speciated Hg Observational Sites Used for Model Evaluation

ID	Site name	Period	Latitude	Longitude	Elev. (m)	Operating agency	Site condition
AI	Appledore Island	May–Oct	42.97	−70.62	18	U New Hampshire	Rural-remote
MD08	Piney Reservoir	Mar–Nov	39.71	−79.01	761	U. of Maryland	Rural-industrial
NH06	Thompson Farm	Mar–Nov	43.11	−70.95	25	U New Hampshire	Rural-remote
NJ05	Brigantine	Mar–Apr	39.46	−74.45	8	St. of New Jersey	Suburban
NY06	New York City	Mar–Nov	40.87	−73.88	26	St. of New York	Urban
NY20	Huntington Wildlife Forest	Mar–Nov	43.97	−74.22	502	Clarkson U.	Rural-remote
NY43	Rochester	Mar–Nov	43.15	−77.62	154	Clarkson U.	Suburban
OH02	Athens	Mar–Nov	39.31	−82.12	274	Ohio Un.	Rural-industrial
VT99	Underhill	Mar–Nov	44.53	−72.87	399	Ecosystem Research Group	Rural-remote
WV99	Canaan Valley Institute	Mar–May	39.12	−79.45	985	NOAA	Rural-remote

Note. Measurement periods below indicate months in 2010.

Mao & Talbot, 2012; Sigler et al., 2009). PBM measurements were only for PM<sub>2.5</sub>; therefore, we used the modeled sum of Aitken and accumulation mode PBM for comparison. Units of GEM and GOM concentrations were converted to ppqv (1 pg m<sup>-3</sup> ≈ 0.12 ppqv for a standard atmosphere) for this evaluation. As these atmospheric Hg measurements were usually 3 h averages, hourly modeled GEM, GOM, and PBM were averaged over 3 h accordingly.

Recent laboratory experiments and reviews (Gustin et al., 2015; Huang & Gustin, 2015; Jaffe et al., 2014; Lyman et al., 2010; McClure et al., 2014) reported measured GOM could be biased due to O<sub>3</sub> and relative humidity (RH) interferences on mercury halides for a KCl-coated denuder, the part of the Tekran 1130 unit commonly used for field measurements. Gustin et al. (2015) suggested to add up measured GOM and PBM together as RM for model evaluation. Even if models may not perfectly reproduce observations, simulated GOM and PBM need to be examined separately to understand our current knowledge of each individual reaction and process in mercury cycling (e.g., chemistry, gas-particle partitioning, and deposition). The information derived from model simulations and sensitivity studies could provide insight into how the mechanisms work. Considering these reasons, in addition to evaluation of GEM, GOM, PBM, RM (i.e., GOM + PBM) evaluation was conducted when valid observations of both GOM and PBM were available.

Biweekly total Hg wet deposition and precipitation depth measurements were obtained from 38 monitor sites of the Mercury Deposition Network (MDN; <http://nadp.sws.uiuc.edu/MDN/>) operated under the National Atmospheric Deposition Program (NADP; Vermette et al., 1995). Simulated hourly wet deposition and precipitation depth data in grid cells containing the MDN sites were summed for biweekly totals to match the observation time intervals. Volume-weighted mean (VWM) Hg concentrations in precipitation were calculated for both observations and simulations. Monthly total Hg wet deposition and monthly average Hg concentrations in precipitation were calculated based on the fraction of each biweekly measurement period for a given month; reported zero values of wet deposition and precipitation were included in the calculations.

To evaluate simulated Hg dry deposition, the results were compared with previous measurements and modeling studies. Wang (2012) estimated growing season Hg dry deposition at NY20 during 2004–2006 using litterfall and throughfall measurements obtained from Bushey et al. (2008) and Choi et al. (2008), respectively. Hg dry deposition was calculated as litterfall Hg plus net throughfall Hg (throughfall – precipitation; Wang, 2012). Litterfall measurements at 11 MDN sites presented by Risch et al. (2017) for 2007–2014 were also used for evaluation. Our results were also compared with the big leaf model studies of Zhang et al. (2012b, 2016a) for 11 AMNet and MDN sites.

Statistical metrics (Chang & Hanna, 2004; Hanna, 1988; Hanna et al., 1991a, 1991b, 1991c, 1993) used to gauge model performance included mean concentrations, coefficient of determination ( $R^2$ ), model mean bias (MB), fractional bias (FB), mean error (ME), normalized mean bias (NMB), and normalized mean error (NME):

$$MB = \overline{C_p} - \overline{C_o}, \quad (1)$$

$$FB = (\overline{C_p} - \overline{C_o}) / 0.5(\overline{C_o} + \overline{C_p}), \quad (2)$$

$$ME = |\overline{C_p} - \overline{C_o}|, \quad (3)$$

$$NMB = (\overline{C_p} - \overline{C_o}) / \overline{C_o}, \quad (4)$$

$$NME = |\overline{C_p} - \overline{C_o}| / \overline{C_o}, \quad (5)$$

where  $C_p$  is model predictions,  $C_o$  is observations, overbar ( $\overline{\phantom{x}}$ ) is average over the data set.

### 3. Results and Discussion

#### 3.1. Modeled Surface Speciated Mercury and Hg Deposition

The spatial distribution of the 9 month average concentrations of GEM, GOM, PBM, and RM surface simulated for the four cases, DEF, DEF\_GS, NEW\_noOH, and NEW are plotted with 9 month mean measurement data at observational sites in Figure 3. These cases exhibited very similar spatial patterns for surface GEM,

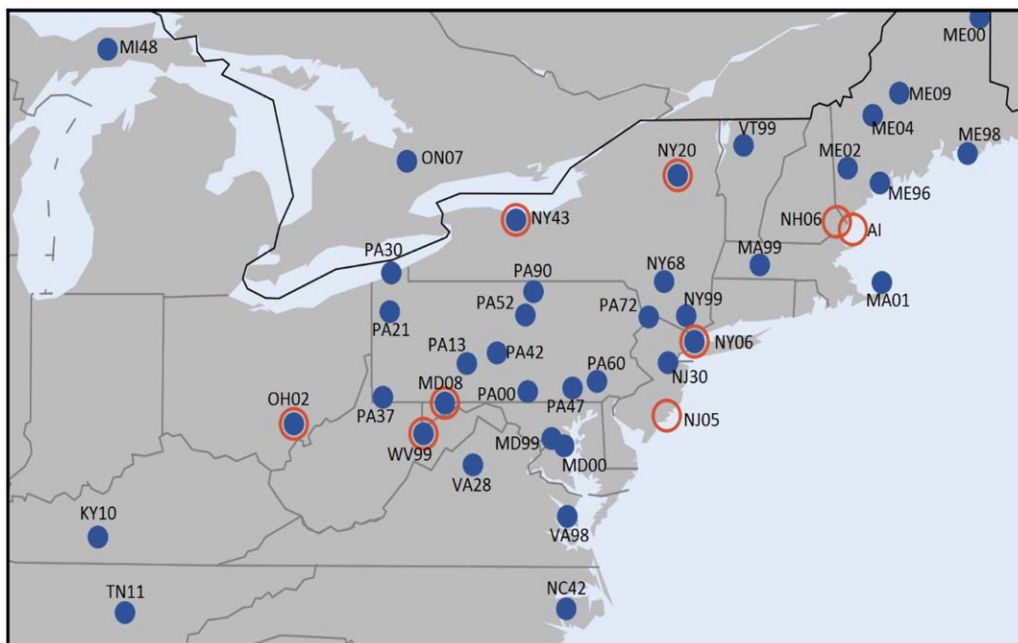


**Figure 3.** Average surface GEM (in ppqv), GOM (in ppqv), PBM (in  $\text{pg m}^{-3}$ ), and RM (in ppqv) mixing ratios estimated from DEF, DEF\_GS, NEW\_noOH, and NEW cases during March–November 2010. The circles indicated observed values at each monitoring site.

GOM, PBM, and RM with differences in magnitude. In particular, modeled surface GEM mixing ratios were significantly impacted by GEM BCs (Figures 3a and 3b). Surface GOM in the three cases constrained by the GEOS-Chem BCs did not differ as much as simulated surface PBM and RM did. Adding GOM and PBM together, RM spatial variation seemed to be controlled mainly by surface PBM. With significantly larger GEM simulated, the DEF\_GS case showed overall overestimation at most of observational sites. The other three cases, however, showed overall underestimation at all sites averaged over the 9 month simulations. Corresponding to overestimated GEM, the DEF case also overestimated GOM, PBM, and RM surface concentrations. GEM surface concentrations in the DEF\_GS, NEW\_noOH, and NEW cases were very close between them, but PBM and RM concentrations in the NEW\_noOH case showed the best agreement with observations. Detailed evaluations will be discussed in section 3.2.

The DEF case used CMAQ-Hg’s default ICs and BCs, whereas the other three cases used GEOS-Chem output as ICs and BCs. As a result, in the DEF case the surface domain and time averaged GEM mixing ratios were significantly larger ( $\sim 36$  ppqv, 26%) than those in the other three cases. Differences among the other three cases (i.e., DEF\_GS, NEW\_noOH, and NEW) were much smaller showing  $< 3$  ppqv on average. The remarkable difference in modeled surface GEM mixing ratios between DEF and the other three cases was the result of the BCs. GEM mixing ratios in the CMAQ-Hg’s default BC profile was  $\sim 32$  ppqv larger than the mean value from the GEOS-Chem BCs, close to the  $\sim 36$  ppqv difference between simulated surface GEM in DEF and other three cases. This difference suggests that BCs play a significant role in simulations of GEM, consistent with previous CMAQ-Hg studies (Baker & Bash, 2012; Holloway et al., 2012; Pongprueksa et al., 2008).

The DEF case also predicted 20–140% larger RM concentrations than the other three cases, due to overestimation of GEM. Note that the difference in GOM between the MBL and inland values was significantly larger in the DEF case compared with the other cases (Figures 3e–3h). This difference is most likely the net effect of the significantly overestimating GEM, an underestimate of GOM dry deposition velocity and greater oxidation of GEM in the MBL. In the MBL the GOM dry deposition velocity was about a factor of 4 smaller than that over land. Photochemical GOM production could thus greatly exceed dry depositional loss in the MBL leading to high concentrations of GOM compared to values over land.

The effects of using our new chemical mechanism on GEM, GOM, PBM, and RM simulations were estimated by comparing the simulated concentrations in DEF\_GS with values in NEW\_noOH and NEW. In CMAQ-Hg

simulations (DEF and DEF\_GS), OH dominated daytime GEM oxidation at a rate  $\sim 4$  times faster than  $O_3$ . With our new chemistry mechanism (NEW\_noOH and NEW), Br, BrO, and  $O_3$  oxidized GEM at about the same rate during daytime in the absence of OH (NEW\_noOH) and at a slightly larger rate than that by OH in the NEW case. Averaged over the modeling domain and time, NEW\_noOH simulated a 1.6% (i.e., 2.2 ppqv) decrease in GEM, a 15% (i.e., 0.08 ppqv) decrease in GOM, and a 33% (i.e.,  $4.0 \text{ pg m}^{-3}$ ) decrease in PBM. This discrepancy varied seasonally, with a maximum discrepancy in the summer when solar radiation was greatest. When comparing NEW, which included the OH-initiated GEM oxidation pathway, with the NEW\_noOH case, there were not significant impacts on GEM and GOM but a 112% increase in PBM. Apparently, PBM was more sensitive than GOM to gaseous photochemical oxidation of GEM because in CMAQ-newHg-Br the GEM + OH products were assumed to form PBM.

Spatial distributions of total Hg wet and dry deposition in the four cases are presented in Figure 4. Simulated total Hg wet deposition was nearly comprised of GOM and PBM wet deposition ( $\sim 99.9\%$ ), and total Hg dry deposition was attributed mostly to GEM and GOM dry deposition ( $>97\%$ ). Domain averaged total Hg wet (dry) deposition for the 9 month simulation period was 6.8 (20.0), 4.1 (8.4), 4.1 (5.2), and 11.5 (9.8)  $\mu\text{g m}^{-2}$  in the NEW, NEW\_noOH, DEF\_GS, and DEF cases, respectively. The DEF case showed considerably larger wet deposition, a factor of 2–3 more than the others. Note that the DEF case exhibited Hg wet deposition flux comparable to values in the NEW case in the center of the domain but exceptionally large values in the boundary grids compared to those in other cases (Figures 4a–4d). The large difference ( $472 \text{ ng m}^{-2}$ ,

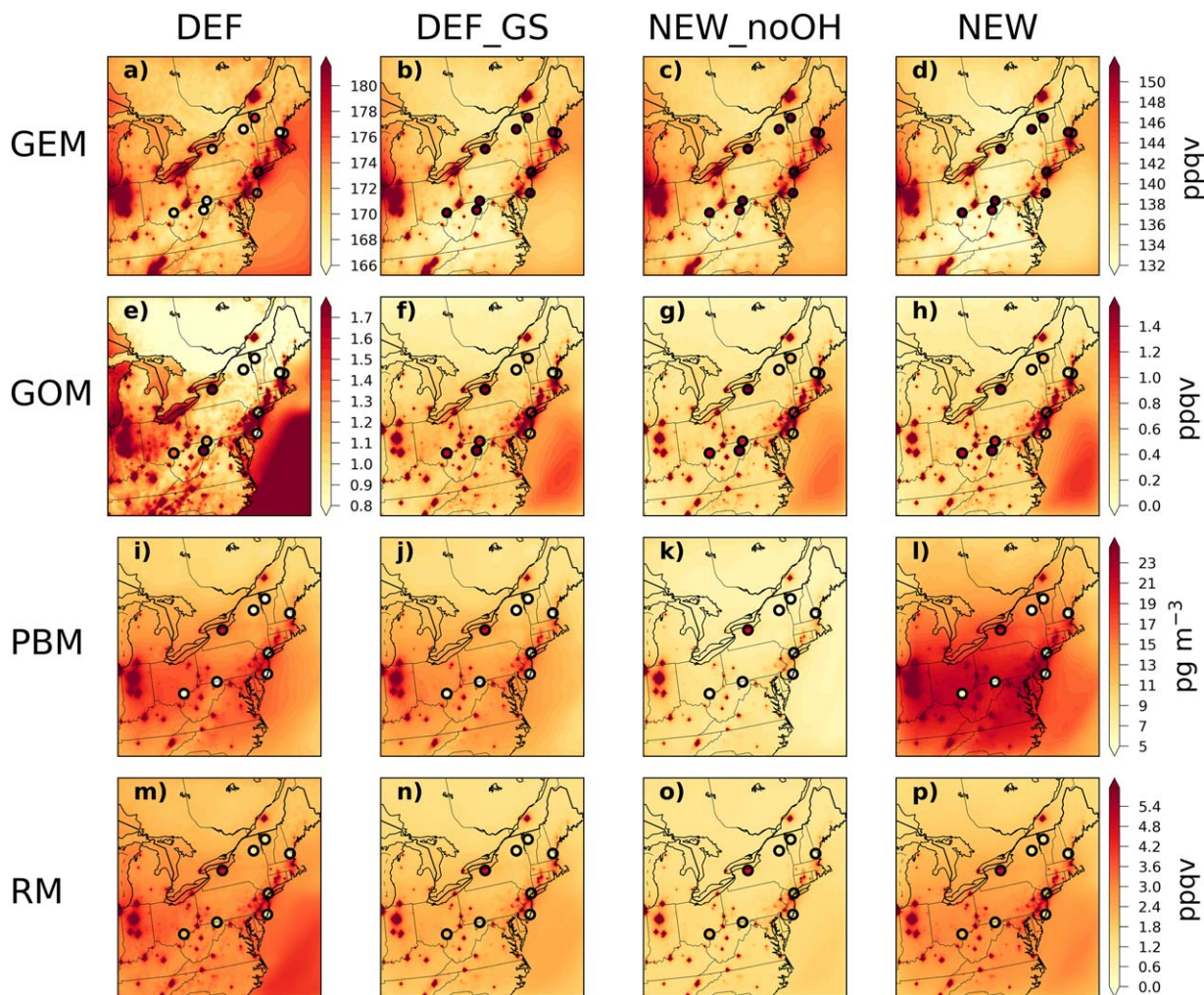


**Figure 4.** Nine-month accumulated total Hg (top) wet and (bottom) dry deposition ( $\mu\text{g m}^{-2}$ ) estimated from DEF, DEF\_GS, NEW\_noOH, and NEW model cases during March–November 2010. The circles indicated observed values at each monitoring site.

75%) in monthly total Hg wet deposition estimates between the DEF and DEF\_GS cases resulted from the default GEM BCs in DEF. This finding is in agreement with Baker and Bash (2012), who also showed that GEM BCs could have significant (20%–99%) contributions to total Hg deposition.

The fraction of Hg dry deposition in total deposition was larger in CMAQ-newHg-Br simulations in the NEW\_noOH and NEW cases (75%) than the CMAQ-Hg simulations in the DEF and DEF\_GS cases (64%). As aforementioned (section 2.1.1), using the new chemistry mechanism, GEM oxidation by O<sub>3</sub> and OH were assumed to take place in solid phase, which likely occurred on land and water surfaces, and the oxidation products of this reaction were lost as Hg dry deposition. This mechanism explains the larger fraction of dry deposition simulated using CMAQ-newHg-Br in NEW and NEW\_noOH (Figures 4g and 4h).

### 3.2. Evaluation of Ambient Mercury Simulations

Using measured-modeled data pairs obtained for the 10 AMNet monitoring sites over the domain, model evaluation metrics were calculated and compared with previous CMAQ-Hg studies (Bieser et al., 2014; Holloway et al., 2012; Table 3). In previous studies (Table 3), surface GEM was simulated reasonably well with NMB of 6%–36%, but surface GOM and PBM were largely overestimated with 220%–970% NMB. In this study, observed mean GEM (164 ppqv) was also simulated reasonably well in all the four cases. The DEF case showed slightly smaller NMB (10%) than that (~–14%) in the other three cases. The average observed ambient GOM concentration (2.5 ppqv) was largely overestimated in the DEF case with NMB of 164%. The other three cases showed better model performance with 2%–9% NMB. The NEW\_noOH case showed the best performance in ambient PBM simulations and RM simulations with the lowest NMB of 20% and 5%, respectively.

#### 3.2.1. Seasonal Variations

Observed-modeled 3 h average concentrations of GEM, GOM, PBM, and RM from the monitoring sites were grouped together by month (Figure 5) to evaluate model performance in seasonal variations. The BCs

**Table 3**

Mean Values and Evaluation Metric for Comparing CMAQ-Hg Sensitivity Simulations From Cases of NEW\_noOH, NEW, DEF\_GS, and DEF With Measurements of GEM, GOM, PBM, and RM at 10 Monitoring Locations in the Domain

Reference Case/site	This study					Holloway et al. (2012)		Bieser et al. (2014) DE02
	Obs	NEW_noOH	NEW	DEF_GS	DEF	DL	MKE	
<i>GEM (ppqv)</i>								
Mean	164	141	139	141	177	180	192	192
MB		–22.6	–24.8	–23.5	12.7	–12.0	–96.0	–12.0
NMB (%)		–14	–15	–14	10	–6	–36	
NME		0.16	0.17	0.17	0.16	0.10	0.36	
FB (%)		–15	–16	–15	7			
<i>GOM (ppqv)</i>								
Mean	1.08	0.99	1.06	1.15	2.46	2.71	4.88	1.32
MB		–0.10	–0.02	0.07	1.40	2.06	3.76	1.13
NMB (%)		–9	–2	6	164	299	331	970
NME		1.17	1.21	1.23	2.16	2.99	3.31	10.10
FB (%)		–9	–2	6	79			
<i>PBM (pg m<sup>–3</sup>)</i>								
Mean	7.6	9.1	19.4	13.5	15.5	29.2	36.2	19.4
MB		1.5	11.8	5.9	7.9	20.9	24.7	9.8
NMB (%)		20	160	80	100	260	220	890
NME		1.5	3.2	2.2	2.6	2.6	2.2	13.8
FB (%)		20	90	60	70			
<i>RM (ppqv)</i>								
Mean	2.1	2.2	3.6	2.9	4.6			
MB		0.1	1.5	0.8	2.5			
NMB (%)		5	71	40	119			
NME		0.9	1.2	1.0	1.6			
FB (%)		5	53	32	75			

Note. In comparison, results from Holloway et al. (2012) at Devil’s Lake (DL) and Milwaukee (MKE) sites, and Bieser et al. (2014) at Waldhof (DE02) site were also shown in the table.

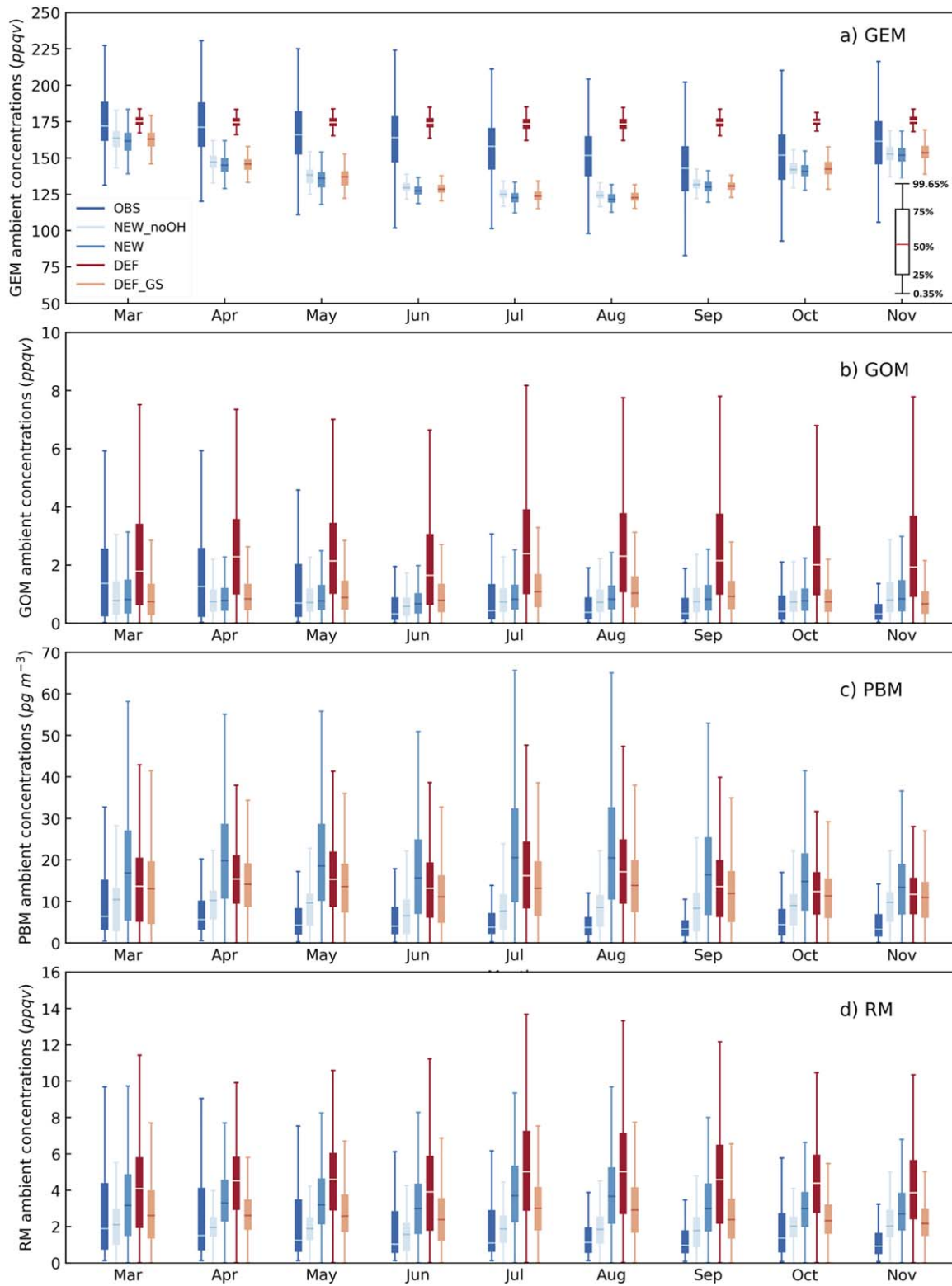


**Figure 5.** Monthly distributions of 2010 observed and modeled hourly ambient (a) GEM, (b) GOM, (c) PBM, and (d) RM mixing ratios at all observatory sites in the model domain.

**Table 4**  
Seasonal Changes of GOM and PBM in Observations and Simulations

Seasonal changes	GOM		PBM	
	Concentration (ppqv)	Percentage	Concentration (pg/m <sup>3</sup> )	Percentage
Observation	0.8	76	2.8	39
NEW	0.4	37	4.2	22
NEW_noOH	0.4	43	2.1	23
DEF_GS	0.2	18	2.1	16
DEF	0.5	18	2.2	15

impact on GEM simulations was clearly shown in the seasonal patterns (Figure 5a). Using constant values for GEM BCs, the DEF case exhibited almost no seasonal variation in GEM. In contrast, the other three cases using GEOS-Chem output for BCs showed distinct seasonal patterns with summertime minimums, 1–2 months ahead of the observed minimum in September. The DEF\_GS, NEW\_noOH, and NEW cases captured the mean observed GEM (154 ppqv, 7% FB) effectively in the fall but underestimated the springtime (169 ppqv, 13% FB) and summertime (157 ppqv, 19% FB) averages. The overall small biases (8–14%) reflected the predominant influence of the BCs from GEOS-Chem output.

Observed ambient GOM, PBM, and RM did not show significant seasonal patterns, but large values often occurred in spring and low values in summer and fall (Figures 5b, 5c, and 5d). NEW\_noOH showed overall best simulations of monthly means with 9% FB for GOM, 20% FB for PBM, and 5% for RM. For further comparison, seasonal changes of GOM and PBM were calculated as the maximum seasonal mean minus the minimum seasonal mean, and percentage changes were calculated as the seasonal change as a percentage of the all-season average (Table 4). Four main characteristics are noted. First, the largest GOM seasonal change was simulated in the DEF case due to the overprediction of GOM. Second, the largest PBM seasonal change was simulated in the NEW case because all products of the GEM + OH reaction were assumed to deposit to particle surface above the surface layer. Third, the DEF and DEF\_GS cases, constrained with different BCs, produced almost the same seasonal percentage change for both GOM and PBM, indicating that this percentage change was caused by the default chemical mechanism. Fourth, CMAQ-newHg-Br with or without the GEM + OH reaction (NEW and NEW\_noOH) produced twice the magnitude of seasonal variation in GOM than CMAQ-Hg (DEF\_GS). Finally, NEW and NEW\_noOH simulated a ~40% seasonal change in GOM and a 22% change in PBM, which more closely depicted observations than the 18% seasonal change in GOM and 15% change in PBM in the DEF and DEF\_GS cases. These improvements in simulations were caused entirely by the introduction of new Hg chemical mechanism.

### 3.2.2. GOM Diurnal Patterns

Atmospheric GOM observations exhibit a daytime peak at 7 out of the 10 AMNet monitoring sites, and the remaining three sites showed a daily peak in the late afternoon to midnight (NH06) or no noticeable diurnal variation (NY20 and WV99; not shown). However, in all four cases simulated GOM displayed distinct diurnal variation with daytime maximums at one location only, Appledore Island (AI), the only marine site, off the coast of southern New Hampshire, USA (Figure 6, using NEW\_noOH and DEF\_GS to represent CMAQ-newHg-Br and CMAQ-Hg, respectively). At the other six sites, modeled GOM exhibited no apparent or weak diurnal variation. A major difference between the spatial configuration of AI and the other nine sites was that the grid containing AI was treated as water surface in the model whereas the grids with other sites as terrestrial surfaces. Therefore, the different treatments of dry deposition velocity and chemistry in the model for water and land surfaces probably resulted in the distinct diurnal pattern in GOM at AI. Indeed, three MDN sites (MA01 [marine], ME98 [marine], and PA30 [lake]), with which the model grids were also treated as water surface, exhibited distinct diurnal cycles in simulated GOM with daytime maximums. This is because photochemical production of GOM exceeds dry depositional loss over water, as discussed in section 3.1, leading to significant daytime maximums at water surface sites. In contrast, at terrestrial sites, modeled GOM dry deposition velocities exhibited significant daytime maximums averaging 5.1 cm s<sup>-1</sup> and daily minimums averaging 2.9 cm s<sup>-1</sup>, a factor of 4 larger than that over water. Such rapid GOM dry deposition during daytime offsets photochemical production, leading to lower daytime GOM concentrations. Note that GOM dry deposition during daytime was almost a factor of 2 greater than wet deposition at terrestrial sites.

Caution needs to be taken in interpreting the discrepancy in modeled and observed GOM, because it may not be conclusive considering the biases in GOM measurements, such as increased wall loss of GOM due to a temperature drop in sampling line (Gustin et al., 2013; Huang & Gustin, 2015). However, for the AI site the RH interference in GOM measurements was limited as stated in our previous study (Ye et al., 2016).

## 3.3. Hg Deposition Evaluation

### 3.3.1. Hg Wet Deposition

Evaluation metrics (Table 5) were calculated using weekly observed-modeled pairs and were compared with results from previous studies. The NEW\_noOH and DEF\_GS cases underestimated 9 month of

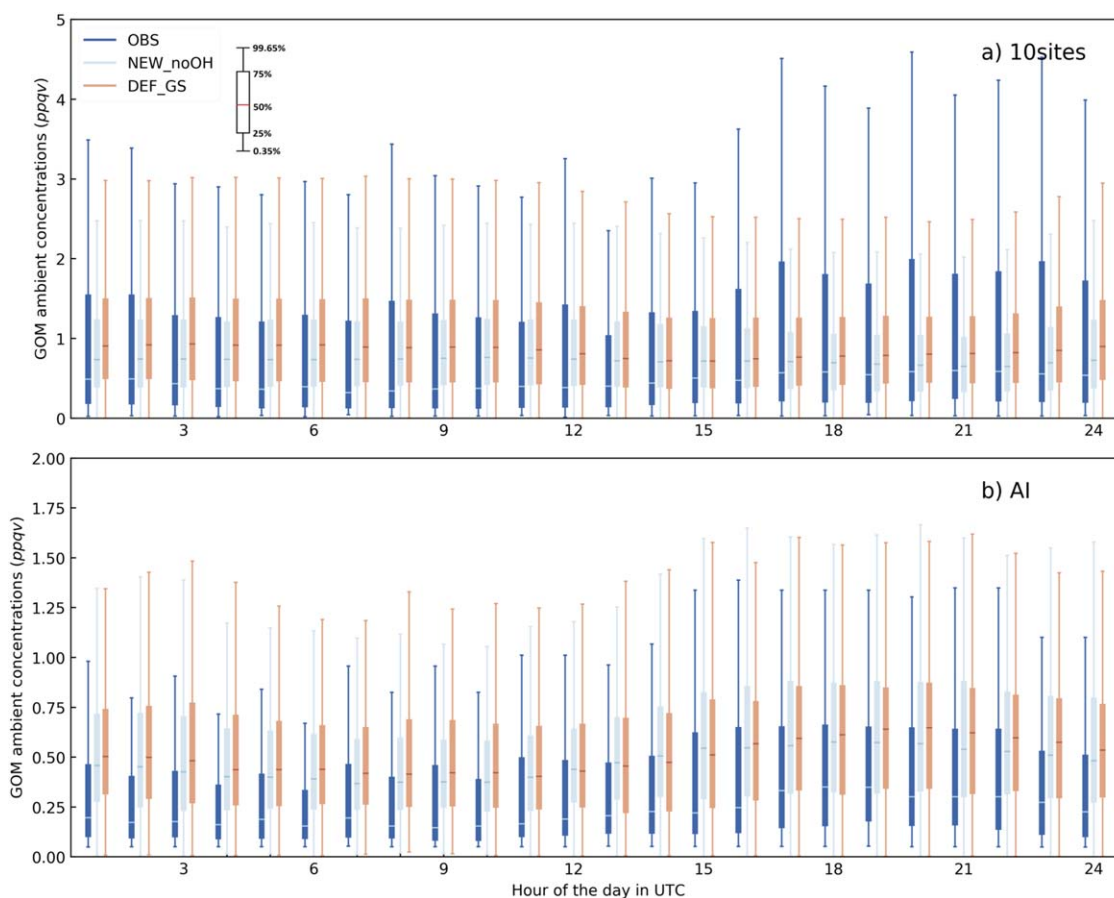


**Figure 6.** Averaged diurnal variation of observed and modeled GOM ambient concentrations (a) at all 10 sites, and at a MBL site, (b) AI for the period of March–November 2010. Local time = UTC – 4:00 for eastern daylight saving time (EDT), and UTC – 5:00 for eastern standard time (EST).

measured total Hg wet deposition by 48% and 45%, respectively. The DEF case overestimated wet Hg deposition by 27%. The NEW case showed the best model performance with a slight underestimation (NMB = –4%; Table 5). These results appear to be inconsistent with the best simulated GOM and PBM concentrations in the NEW\_noOH case (see section 3.2). An evaluation of WRF simulated precipitation using

**Table 5**  
Evaluation Metric for Comparing CMAQ-Hg Sensitivity Simulations of Weekly Hg Wet Deposition Flux From Cases of NEW\_noOH, NEW, DEF\_GS, and DEF With Measurements at all MDN Sites in the Domain

Reference	Region	MB	FB (%)	ME	NMB (%)	NME	R <sup>2</sup>
This study NEW	NE US	–0.6	–0.4	–104	–4	–0.62	0.29
DEF	NE US	35	19	136	27	0.81	0.23
DEF_GS	NE US	–71	–56	99	–45	0.59	0.28
NEW_noOH	NE US	–76	–62	105	–48	0.63	0.24
Vijayaraghavan et al. (2007)	US				29	0.402	0.41
Bullock et al. (2009)	North American	–12.2		178.1	–5	0.708	0.15
Holloway et al. (2012)	Great Lakes				–21	0.55	0.27
Baker and Bash (2012)	EUS	–171 to 61	–45 to 35	121–253			
Baker and Bash (2012)	WUS	210–467	51–110	295–513			
Myers et al. (2013)	SW US			267–1115	–6 to –47	0.35–0.58	
Lu et al. (2014)	Mid-South US				–49		0.23
Grant et al. (2014)	Great Lakes				62	0.72	
Bieser et al. (2014)	Europe	–30		36			0.91

Note. Evaluation results of other CMAQ-Hg studies were also shown for reference.

MDN precipitation depth data suggested a 12% underestimation at all sites, which could partially explain the 48% underestimation of Hg wet deposition in the NEW\_noOH case.

Total Hg wet deposition is supposedly determined by total GOM and PBM integrated in a precipitating layer instead of surface concentrations only. Previous studies reviewed in Mao et al. (2016) showed high GOM concentrations reaching up to 24–82 ppqv in the upper troposphere. Moreover, recent studies by Gratz et al. (2015) and Shah et al. (2016) found GOM reaching hundreds of  $\text{pg m}^{-3}$  at high altitudes. Such high concentrations of GOM in upper air are thought to be due to GEM oxidation by more abundant Br radicals, less loss through deposition, and lower temperature (Brooks et al., 2014; Gratz et al., 2015; Lyman & Jaffe, 2012; Shah et al., 2016; Sillman et al., 2007). Sillman et al. (2007), using the default CMAQ-Hg, reported very similar simulated GOM concentrations to those in our DEF case, showing lower upper air concentrations compared with measurements. However, in our other three cases using GEOS-Chem BCs, estimated upper layer GOM concentrations (Figure 7) were >90% smaller than the observed GOM in Florida reported by Sillman et al. (2007). Another interesting finding was the differences in vertical profiles of GOM and PBM simulated using different chemical mechanisms. We found significantly larger (about a factor of 5) GOM in upper layers simulated in the NEW case compared with that in the DEF\_GS case (Figure 7). This difference was likely attributed to stronger oxidation by more abundant Br at higher altitudes simulated in the NEW case. The vertical distribution of PBM in the NEW case showed higher surface concentrations than those in the upper layers compared with those in the DEF\_GS case. These GOM and PBM differences may explain the better simulated Hg wet deposition in the NEW case. Nonetheless, since vertical GOM profile measurements are not available for our modeling domain, a comparison between our results and previous studies remains unresolved. However, the good agreement between modeled and observed Hg wet deposition and reasonably predictions of precipitation depth indicate that although there appears to be large discrepancy between modeled and measured GOM at certain altitudes, the simulated column total RM may be a sound approach to predict wet Hg deposition.

Also note that the NEW and NEW\_noOH case predicted 16% larger GOM in upper air (>2 km) than the DEF\_GS case. Since these three cases used the same BCs from GEOS-Chem output, this difference in simulation results underscores the importance of using state-of-the-art Hg and Br chemistry in simulations. The NEW and NEW\_noOH cases simulated similar GOM vertical profiles, but Hg wet deposition was better captured (4% bias) in the NEW case. Apparently including the GEM + OH reaction (NEW case) produced more than twice the PBM in the NEW\_noOH case and ultimately yielded better simulated Hg wet deposition. This suggests that including OH-initiated GEM oxidation pathway for PBM formation produced better model simulations in reproducing observed Hg wet deposition. However, it should be noted that the agreement between simulated and observed Hg wet deposition possibly resulted from compensating errors in multiple simulated parameters that control Hg wet deposition flux.

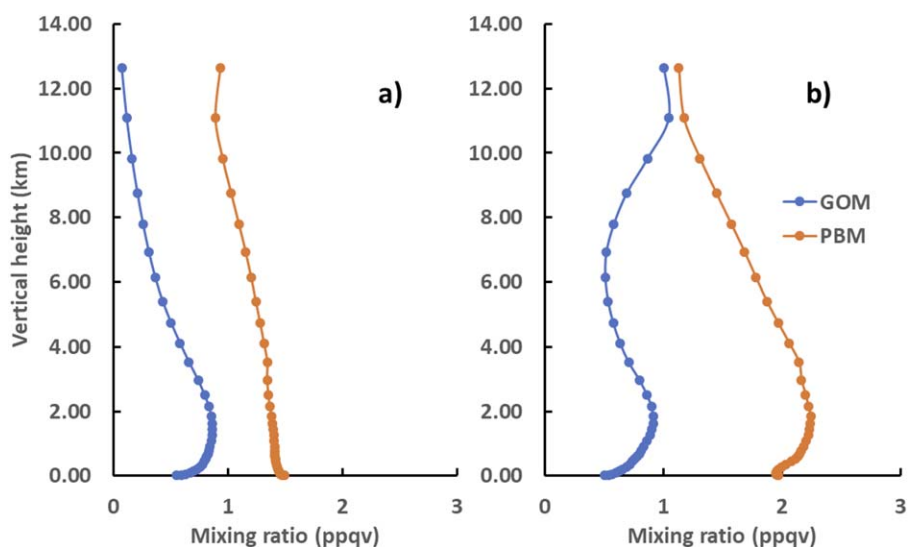
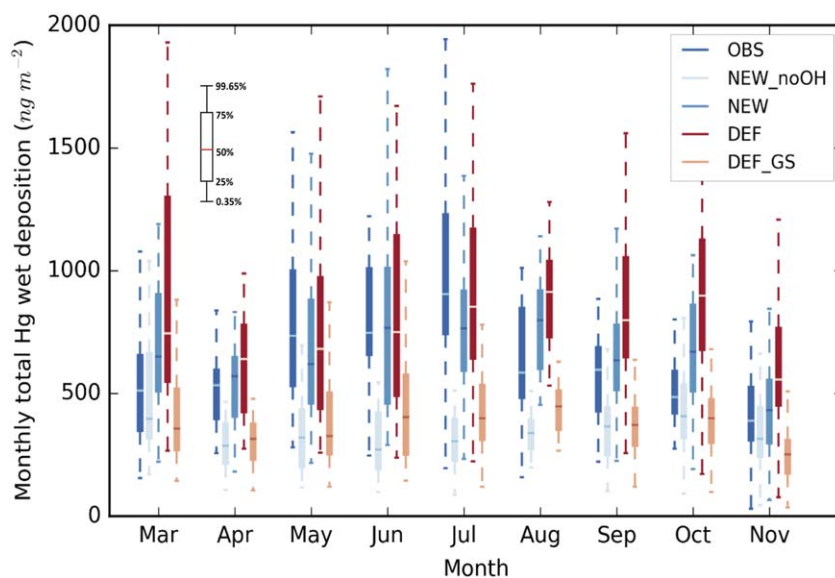
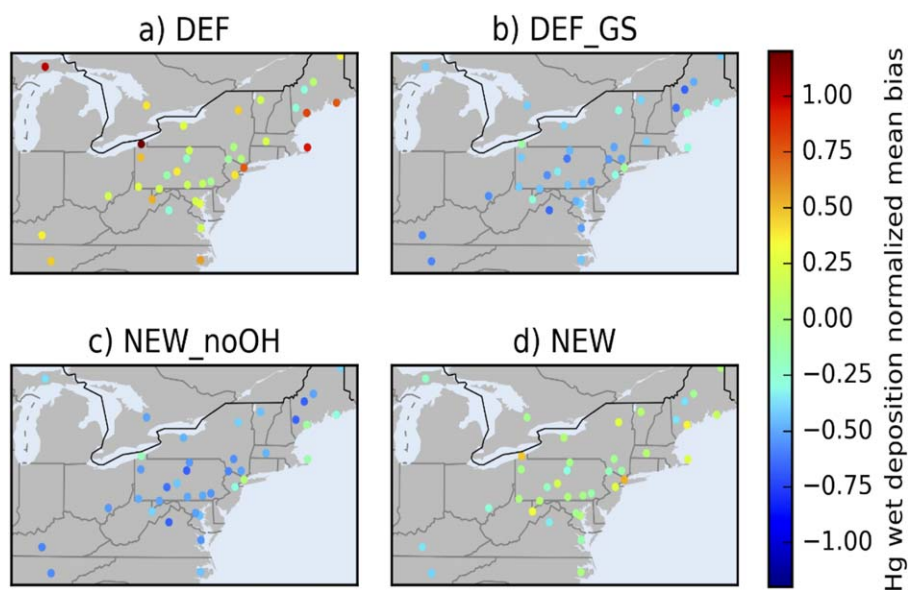


Figure 7. Vertical profiles of simulated GOM and PBM in the (a) DEF\_GS and (b) NEW case.



**Figure 8.** Seasonal variation of observed and simulated monthly total Hg wet deposition for the simulation period of March–November 2010 at 38 MDN sites in the domain.

In addition to the total Hg wet deposition, the observed summertime maximum Hg wet deposition was predicted very well (~3% bias) in the NEW case (Figure 8). In contrast, NEW\_noOH underestimated Hg wet deposition especially in summer but performed well in spring and fall. Holmes et al. (2016) suggested that deep convective thunderstorms could effectively scavenge reactive mercury from the upper troposphere and subsequently enhance Hg concentrations in precipitation. With total estimated precipitation depth of 25.5 cm in spring, 36.9 cm in summer, and 36.0 cm in fall, convective precipitation constituted 9%, 48%, and 7%, respectively, of total precipitation. More convective precipitation in summer combined with potentially underestimated GOM in the upper troposphere probably contributed to the underestimate of wet Hg deposition in summer compared to other seasons in the NEW\_noOH case. As shown in the NMB spatial distributions for Hg wet deposition (Figure 9) and Hg concentrations in precipitation (Figure 10), in the NEW case CMAQ-newHg-Br performed well at almost all sites with an average NMB of -1.5%. In contrast, the



**Figure 9.** Normalized mean bias of four model cases in simulating accumulated total Hg wet deposition at the MDN sites in the domain for the simulation period of March–November 2010.

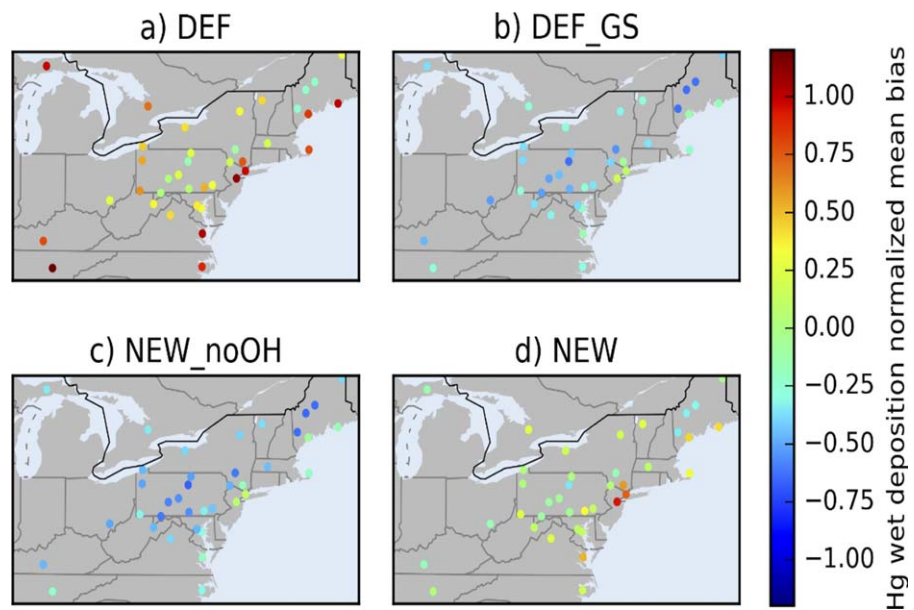


**Figure 10.** Normalized mean bias of four model cases in estimating Hg concentrations in precipitation at all MDN sites in the domain for the period of March–November 2010.

DEF\_GS and NEW\_noOH cases, CMAQ-Hg constrained with BCs from GEOS-Chem output and CMAQ-newHg-Br without GEM + OH underestimated wet Hg deposition at most sites with  $\sim -45\%$  NMB (Table 5). In the DEF case CMAQ-Hg with constant BCs generally overestimated Hg wet deposition with 29% NMB especially at sites near the domain boundaries. At four sites located near the domain boundaries (MI48, KY10, TN11, and NC42), the DEF case exhibited 37–101% NMB for simulated Hg wet deposition, and 79–163% NMB for simulated Hg concentrations in precipitation. The overestimated Hg wet deposition and Hg concentrations in precipitation at sites near the domain boundaries in the DEF case were most likely caused by the use of the default BCs with constant values.

### 3.3.2. Hg Dry Deposition

Estimates of total Hg dry deposition in this study were compared with previous studies (Table 6). Since the DEF case significantly overestimated ambient concentrations of GEM and GOM (see section 3.2) conceivably resulting in unusually large Hg dry deposition, this case was excluded in evaluation of modeled dry deposition.

Modeled Hg dry deposition in the three cases was compared with Zhang et al. (2012b, 2016a), who used the inferential method that combined observed speciated Hg concentrations with dry deposition velocities simulated using a big leaf model. At the 10–11 of the common sites studied (Table 6), Zhang et al. (2012b) estimated an annual dry deposition varying over  $5.2\text{--}26.1 \mu\text{g m}^{-2}$  during 2008–2009. Zhang et al. (2016a) estimated  $3.1\text{--}18.7 \mu\text{g m}^{-2}$  on average over 2009–2014. For the same sites, we simulated total Hg dry deposition during March to November 2010 for the NEW, NEW\_noOH, and DEF\_GS cases in the range of  $19.6\text{--}44.0$ ,  $8.9\text{--}20.6$ , and  $6.3\text{--}11.3 \mu\text{g m}^{-2}$ , respectively. For an urban site, NY06, in New York City we simulated exceptionally high dry deposition of  $83.6$ ,  $65.5$ , and  $31.8 \mu\text{g m}^{-2}$  in the NEW, NEW\_noOH, and DEF\_GS cases, respectively, due to very high GEM and GOM concentrations due to heavy anthropogenic emissions. Generally, total Hg dry deposition estimated in the NEW\_noOH and DEF\_GS cases were in good agreement with Zhang et al. (2012b, 2016a).

The differences between Hg dry deposition estimated using CMAQ and the inferential method are likely due to the following reasons: (1) different mechanisms were used in calculating dry deposition velocities. A bidirectional exchange mechanism was used in our CMAQ simulations to calculate GEM dry deposition and the M3DRY mechanism was used to calculate GOM and PBM dry deposition velocities. Zhang et al. (2012b, 2016a) calculated dry deposition velocities using the big leaf model for all speciated Hg species. (2) In CMAQ simulations, dry deposition velocities were calculated for each  $12 \text{ km} \times 12 \text{ km}$  grid cell, instead of

**Table 6**  
*Simulated Accumulated Hg Dry Deposition During March–November 2010 by the Model Cases in This Study, and Compared With Annual Hg Dry Deposition Estimation From Zhang et al. (2012b, 2016a), and Litterfall Measurements From Risch et al. (2017)*

Site	This study			Zhang et al. (2016a) <sup>a</sup>	Zhang et al. (2012b) <sup>a</sup>	Risch et al. (2017)
	NEW_noOH	NEW	DEF_GS			
KY10	11.6	27	7.7			12.6 ± 0.1
MD08	10.8	22.5	7.9	10.5	14.9	15.3 ± 2.1
MD99	11.6	27	7.7	12.5	10.6	14.6 ± 1.9
MI48	6.9	16.1	5.1			6.2 ± 1.1
NH06	13.4	33.0	7.8	7.7	21.2	
NJ05	18.4	44.0	9.7	18.7	26.1	
NJ30	20.6	36.6	11.3		23.9	
NY06	65.5	83.6	31.8	8.0	9.2	
NY20	10.6	19.6	7.4	10.8	5.2	11.2 ± 0.6
NY43	13.6	28.1	8.1	8.5	13.8	
NY68	12.4	24.3	8.8			12.2 ± 3.6
OH02	8.9	21.0	6.3	4.5	13.3	18.8 ± 2.8
PA13	11.0	24.0	8.3			13.4 ± 2.1
PA30	3.6	14.6	0.8			14.6 ± 0.8
PA42	9.1	19.7	6.6			7.5 ± 0.04
TN11	8.0	16.2	6.1			14.9 ± 4.7
VA28	9.4	20.2	6.3			7.8 ± 0.8
VT99	11.6	21.5	8.0	9.0	12.7	11.3 ± 1.8
WV99	12.1	23.1	9.1	3.1	12.2	9.3 ± 1.0

Note. Unit:  $\mu\text{g m}^{-2}$ .

<sup>a</sup>Zhang et al. (2012b, 2016a) presented annual total Hg dry deposition fluxes, not 9 months fluxes in this study.

for a monitoring site as done in Zhang et al. (2012b, 2016a). (3) Concentrations of Hg species from simulations in CMAQ were used to calculate dry Hg deposition, which could differ from observed concentrations used in Zhang et al. (2012b, 2016a).

In addition, our simulated dry deposition flux was compared with values estimated using litterfall and throughfall measurements. Since GOM and PBM can contribute to litterfall Hg (Risch et al., 2012, supporting information), total Hg dry deposition, instead of dry deposition of GEM only as in Wang (2012), was compared with the litterfall Hg measurements. Wang (2012) estimated  $16.5 \mu\text{g m}^{-2}$  Hg dry deposition based on litterfall and throughfall measurements during the 2004–2006 growing season (May–October) at the Huntington Wildlife Forest site (NY20). During the same months, 12.9, 7.0, and  $5.1 \mu\text{g m}^{-2}$  Hg dry deposition was simulated in the NEW, NEW\_noOH, and DEF\_GS cases, respectively, about 20%–70% lower than values estimated by Wang (2012). Our simulated 2010 Hg dry deposition was smaller than the simulated values for 2004–2006 in Wang (2012) due possibly to significant decreases in anthropogenic Hg emissions, which were also thought to have led to the observed Hg concentrations over North America during this period (e.g., Weiss-Penzias et al., 2016; Zhang et al., 2016b). Hg dry deposition estimated in the NEW case was also the closest to litterfall Hg reported by Bushey et al. (2008) at the same site for 2004 ( $17.9 \mu\text{g m}^{-2}$ ) and 2005 ( $16.4 \mu\text{g m}^{-2}$ ). Risch et al. (2017) presented Hg deposition via litterfall at additional MDN sites. At most MDN sites, the Hg dry deposition simulated in NEW\_noOH was in close agreement with that in Risch et al. (2017) with NMB of  $-19\%$ , whereas values in NEW differed significantly varying over 0–90% with an overall NMB of 75% (Table 6). If litterfall is considered as the low end of Hg dry deposition (Wright et al., 2016), total Hg dry deposition flux simulated using CMAQ-newHg-Br without the GEM + OH reaction appeared to be more reasonable than using the default CMAQ-Hg.

Simulation of total Hg dry deposition remains challenging and has large uncertainties due to a lack of direct measurements, uncertainties in modeled dry deposition velocities of speciated Hg, and poor knowledge of Hg chemistry and speciation (Wright et al., 2016; Zhang et al., 2016a). In our model simulations, GEM and GOM contributed to nearly all (>98%) of total Hg dry deposition, to which GEM deposition contributed 34% in NEW\_noOH and 15% in NEW, markedly lower than the 54% in DEF\_GS. In comparison, a higher fraction of GEM in total Hg dry deposition, of 46–96% was estimated in Zhang et al. (2012b) and 97.5% in Yu et al. (2013). This discrepancy was mainly due to differences in dry deposition velocities, very low (sometimes

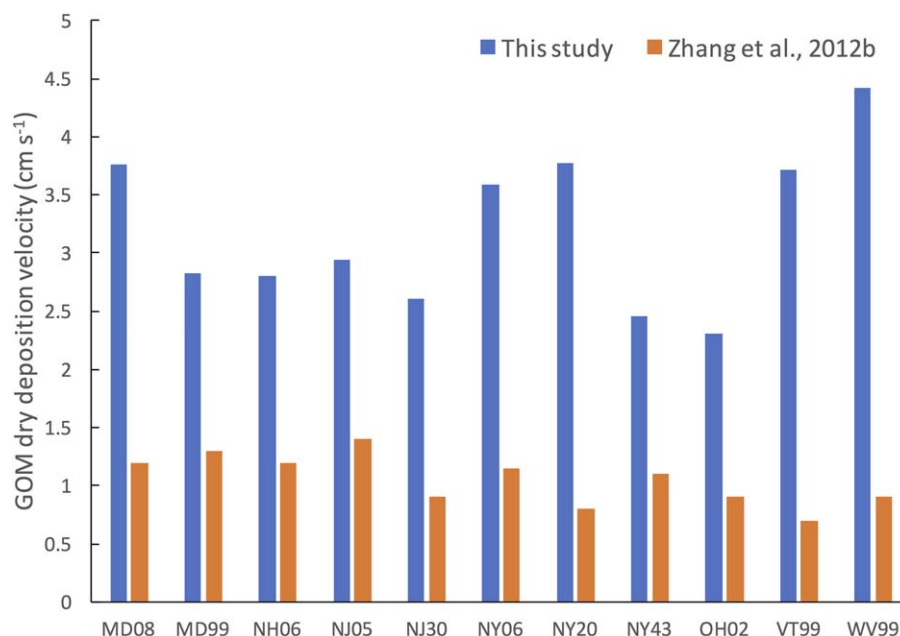


**Figure 11.** Simulated GOM dry deposition velocity ( $\text{cm s}^{-1}$ ) averaged for the 9 month period in NEW case (blue) and annual average values from Zhang et al. (2012b).

lower than the detection limit) measured GOM ambient concentrations, and our consideration of surface GEM oxidation. Specifically, GOM dry deposition velocities simulated in our study (Figure 11) were about a factor of 2 larger than the estimates of the big leaf dry deposition model (Zhang et al., 2012b). Also, the dry deposition products of GOM from GEM + OH/O<sub>3</sub> comprised 31% and 65%, respectively, of total dry deposition in the NEW and NEW\_noOH cases.

Zhang et al. (2012a) compared CMAQ-Hg simulated daytime and nighttime dry deposition flux against short-term surrogate surface observations and found reasonable model-observation agreement at night but overprediction of GOM + PBM dry deposition by a factor of 5 during daytime. Based on our finding that significantly high GOM dry deposition velocities were simulated during daytime compared to the night (see section 3.2.2), overpredicted daytime dry depositional loss of GOM could be one of the main reasons why CMAQ-Hg did not reproduce the observed GOM diurnal cycle.

#### 4. Summary

In this study, CMAQ-Hg, a commonly used regional photochemical transport model, was modified by implementing a state-of-the-art mercury and halogen chemical mechanism. The modified model, named CMAQ-newHg-Br, was evaluated against long-term measurement data at monitoring sites in the Northeast U.S. Compared to the OH-dominated GEM oxidation mechanism in CMAQ-Hg model, Br-induced gas-phase oxidation of GEM in CMAQ-newHg-Br resulted in lower near surface GOM (18%) and PBM (33%) concentrations and improved model performance of GOM and PBM with bias of 2% and 18%, respectively. Moreover, greater seasonal changes of GOM and PBM were simulated using CMAQ-newHg-Br compared with a lack of seasonal change using CMAQ-Hg. The diurnal pattern of GOM with a daytime maximum was captured at water surface sites only due to GOM photochemical production dominant over the low dry depositional loss. Diurnal variation in GOM was not captured for terrestrial sites likely due to an overestimation of daytime GOM dry deposition velocities over land. The inclusion of Br chemistry in CMAQ-newHg-Br enhanced column GOM concentrations by 14% and resulted in 16% increase in GOM wet deposition compared to simulations in the DEF\_GS case that employed the CMAQ-Hg's default OH oxidation mechanism. Including GEM oxidation by OH as a gas-phase reaction with solid products produced on Earth's and aerosol surface in CMAQ-newHg-Br remarkably improved the simulation of Hg wet deposition with average  $-1.5\%$  NMB for all the MDN sites in the domain. In addition, compared to CMAQ-Hg, CMAQ-newHg-Br simulated total

Hg dry deposition in closer agreement with values estimated using inferential method and litterfall/throughfall measurements.

This study demonstrates that Br chemistry should be explicitly depicted in regional atmospheric Hg models. GEM oxidation products initiated by O<sub>3</sub> and OH should be treated with caution due to impacts on ambient GOM and PBM concentrations as well as Hg wet and dry deposition simulations. GEM BCs have significant impacts on simulated atmospheric Hg concentrations and deposition. It is recommended that time-dependent BCs should be used rather than constant BCs in regional simulations. It would be ideal to use CMAQ-Hg's continental U.S. simulations to constrain our Northeastern U.S. simulations, which would make the results more consistent. This is one area that could potentially be improved in the future. Also, kinetic data for HgBr reactions were updated most recently (Jiao & Dibble, 2017). Due to the limited time frame of the funded project, it was not possible to rerun all the cases in this study. However 3 month sensitivity simulations conducted using these new rate coefficients for G15-G23 (Table A1) suggested <10% changes in GOM concentrations and negligible effects on GEM and PBM concentrations. CMAQ-newHg-Br will continue to be improved by incorporating evolving knowledge of atmospheric Hg chemistry, better and more complete emission inventories, better estimates of GOM dry deposition velocities, and a more realistic parameterization of gas-particle partitioning. This model can ultimately be used, with confidence, to quantify the sources/sinks and processes that control atmospheric Hg budgets and provide reliable scientific input for future emission control strategies.

### Appendix A: Gas Phase Hg and Br Reactions in the Model

The gas phase Hg and Br reactions implemented in the CMAQ-newHg-Br model were shown in Table A1 and Table A2, respectively.

**Table A1**  
Gas-Phase Hg Reactions Used in New Mechanism

No.	Reactions	Kinetic (cm <sup>3</sup> molecule <sup>-1</sup> s <sup>-1</sup> )	Reference
G1	Hg + O <sub>3</sub> → HgO(s) + O <sub>2</sub>	3.0 × 10 <sup>-20</sup>	Hall (1995)
(G2)	Hg + OH {+O <sub>2</sub> } → HgO(s) + HO <sub>2</sub>	3.55 × 10 <sup>-14</sup> e <sup>294/T</sup>	Pal and Ariya (2004)
G3	Hg + H <sub>2</sub> O <sub>2</sub> → Hg(OH) <sub>2</sub>	8.5 × 10 <sup>-19</sup>	Tokos et al. (1998)
G4	Hg + Cl → HgCl	2.2 × 10 <sup>-32</sup> e <sup>680(1/T - 1/298)}</sup> × [M]	Donohoue et al. (2005)
G5	Hg + Cl <sub>2</sub> → HgCl <sub>2</sub>	2.6 × 10 <sup>-18</sup>	Ariya et al. (2002)
G6	Hg + Br → HgBr	3.7 × 10 <sup>-13</sup> (T/298) <sup>-2.76</sup>	Goodsite et al. (2004, 2012) <sup>a</sup>
G7	Hg + BrO → HgBrO <sup>b</sup>	1.8 × 10 <sup>-14</sup>	Raofie and Ariya (2004)
G8	HgBr → Hg + Br	1.6 × 10 <sup>-9</sup> (T/298) <sup>1.86</sup> e <sup>-7801/T</sup> × [M] <sup>c</sup>	Dibble et al. (2012)
G9	HgBr + Br → Hg + Br <sub>2</sub>	3.89 × 10 <sup>-11</sup>	Balabanov et al. (2005)
G10	HgBr + Br → HgBr <sub>2</sub>	2.98 × 10 <sup>-11</sup>	Balabanov et al. (2005)
G11	ClO + HgCl → ClHgOCl	5.0 × 10 <sup>-11</sup>	Dibble et al. (2012) <sup>d</sup>
G12	ClO + HgBr → BrHgOCl	5.0 × 10 <sup>-11</sup>	Dibble et al. (2012) <sup>d</sup>
G13	BrO + HgCl → BrHgOCl	1.09 × 10 <sup>-10</sup>	Dibble et al. (2012) <sup>e</sup>
G14	BrO + HgBr → BrHgOBr	1.09 × 10 <sup>-10</sup>	Dibble et al. (2012), Wang et al. (2014)
G15	NO <sub>2</sub> + HgCl → ClHgNO <sub>2</sub>	8.6 × 10 <sup>-11</sup>	Dibble et al. (2012) <sup>d</sup>
G16	NO <sub>2</sub> + HgBr → BrHgONO	8.6 × 10 <sup>-11</sup>	Dibble et al. (2012) <sup>d</sup>
G17	HO <sub>2</sub> + HgCl → ClHgOOH	8.2 × 10 <sup>-11</sup>	Dibble et al. (2012) <sup>e</sup>
G18	HO <sub>2</sub> + HgBr → BrHgOOH	8.2 × 10 <sup>-11</sup>	Dibble et al. (2012), Wang et al. (2014)
G19	OH + HgCl → ClHgOH	6.33 × 10 <sup>-11</sup>	Dibble et al. (2012) <sup>e</sup>
G20	OH + HgBr → BrHgOH	6.33 × 10 <sup>-11</sup>	Dibble et al. (2012), Wang et al. (2014)

<sup>a</sup>Hynes et al. (2009) suggested that the reaction of HgBr + Br (G11) could produce an underestimation of the rate coefficient obtained by Donohoue et al. (2006). We used Goodsite et al. (2004, 2012) rate coefficient for Hg + Br instead of the one from Donohoue et al. (2006). <sup>b</sup>The mechanism of this reaction is currently unclear but was included because experimental studies (Raofie & Ariya, 2003, 2004; Spicer et al., 2002) did observe GEM loss due to BrO. <sup>c</sup>Unit for rate coefficients of G8 is s<sup>-1</sup>. <sup>d</sup>The rate coefficients were suggested by T. Dibble (personal communication, 2013). <sup>e</sup>The rate coefficients of these HgCl reactions were not included in Dibble et al. (2012), they were assumed as the same kinetic as the HgBr reactions, which were calculated by Wang et al. (2014).

**Table A2**  
Gas-Phase Br Reactions Used in New Mechanism

No.	Reactions	Kinetic (cm <sup>3</sup> molecule <sup>-1</sup> s <sup>-1</sup> )	Reference
BR1	Br <sub>2</sub> → 2Br	Photolysis	
BR2	BrO → Br + O	Photolysis	
BR3	HOBr → Br + OH	Photolysis	
BR4	BrONO <sub>2</sub> → BrO + NO <sub>2</sub>	Photolysis	
BR5	BrONO <sub>2</sub> → Br + NO <sub>3</sub>	Photolysis	
BR6	BrNO <sub>2</sub> → Br + NO <sub>2</sub>	Photolysis	
BR7	CHBr <sub>3</sub> → CHBr <sub>2</sub> + Br	Photolysis	
BR8	BrCl → Br + Cl	Photolysis	
BR9	BrOO → BrO + O	Photolysis	
BR10	BrOO + NO → BrO + NO <sub>2</sub>	$2.37 \times 10^{-13} e^{607/T}$	Li et al. (2002)
BR11	Br + BrOO → 2BrO	$5.0 \times 10^{-12}$	Sander and Watson (1981)
BR12	BrO + BrO → 2Br + O <sub>2</sub>	$2.4 \times 10^{-12} e^{40/T}$	Sander et al. (2006)
BR13	BrO + BrO → Br <sub>2</sub> + O <sub>2</sub>	$2.8 \times 10^{-14} e^{860/T}$	Sander et al. (2006)
BR14	BrO + ClO → Br + OClO	$9.5 \times 10^{-13} e^{550/T}$	Sander et al. (2006)
BR15	BrO + ClO → Br + ClOO	$2.3 \times 10^{-12} e^{260/T}$	Sander et al. (2006)
BR16	BrO + ClO → BrCl + O <sub>2</sub>	$4.1 \times 10^{-13} e^{290/T}$	Sander et al. (2006)
BR17	BrO + HO <sub>2</sub> → HOBr + O <sub>2</sub>	$4.5 \times 10^{-12} e^{500/T}$	Atkinson et al. (2006)
BR18	BrO + NO → Br + NO <sub>2</sub>	$8.7 \times 10^{-12} e^{260/T}$	Atkinson et al. (2007)
BR19	BrO + NO <sub>2</sub> → BrONO <sub>2</sub>	$k_0 = 5.2 \times 10^{-31} (T/300)^{-3.2}$ , $k_\infty = 6.9 \times 10^{-12} (T/300)^{-2.9}$ ; $F = 0.6$ and $N = 1.0$	Sander et al. (2006)
BR20	BrO + O → Br + O <sub>2</sub>	$1.9 \times 10^{-11} e^{230/T}$	Sander et al. (2006)
BR21	BrO + OH → Br + HO <sub>2</sub>	$1.8 \times 10^{-11} e^{250/T}$	Atkinson et al. (2007)
BR22	Br + HO <sub>2</sub> → HBr + O <sub>2</sub>	$4.8 \times 10^{-12} e^{310/T}$	Sander et al. (2006)
BR23	Br + NO <sub>2</sub> → BrNO <sub>2</sub>	$k_0 = 4.2 \times 10^{-31} (T/300)^{-2.4}$ , $k_\infty = 2.7 \times 10^{-11} (T/300)^{0.0}$ ; $F = 0.6$ and $N = 1.0$	Sander et al. (2006)
BR24	Br + BrONO <sub>2</sub> → Br <sub>2</sub> + NO <sub>3</sub>	$4.9 \times 10^{-11}$	Orlando and Tyndall (1996)
BR25	Br + NO <sub>3</sub> → BrO + NO <sub>2</sub>	$1.6 \times 10^{-11}$	Mellouki et al. (1989)
BR26	Br + O <sub>3</sub> → BrO + O <sub>2</sub>	$1.7 \times 10^{-11} e^{-800/T}$	Sander et al. (2006)
BR27	Br <sub>2</sub> + OH → HOBr + Br	$2.1 \times 10^{-11} e^{240/T}$	Sander et al. (2006)
BR28	HBr + OH → Br + H <sub>2</sub> O	$5.5 \times 10^{-12} e^{200/T}$	Sander et al. (2006)
BR29	HBr + O → OH + Br	$5.8 \times 10^{-12} e^{-1,500/T}$	Sander et al. (2006)
BR30	HOBr + O → OH + BrO	$1.2 \times 10^{-10} e^{-430/T}$	Sander et al. (2006)
BR31	BrONO <sub>2</sub> + O → NO <sub>3</sub> + BrO	$1.9 \times 10^{-11} e^{215/T}$	Sander et al. (2006)
BR32	Br + OClO → BrO + ClO	$2.6 \times 10^{-11} e^{-1,300/T}$	Sander et al. (2011)
BR33	BrO + NO <sub>3</sub> → BrOO + NO <sub>2</sub>	$1.0 \times 10^{-12}$	Sander et al. (2011)
BR34	Br + HCHO → HBr + HCO	$1.7 \times 10^{-11} e^{-800/T}$	Sander et al. (2006)
BR35	Br + CH <sub>3</sub> CHO → HBr + CH <sub>3</sub> CO	$1.8 \times 10^{-11} e^{-460/T}$	Atkinson et al. (2006)
BR36	Br + C <sub>2</sub> H <sub>4</sub> → BrC <sub>2</sub> H <sub>4</sub>	$1.3 \times 10^{-13}$	Atkinson et al. (2006)
BR37	Br + C <sub>3</sub> H <sub>6</sub> → BrC <sub>3</sub> H <sub>6</sub>	$3.6 \times 10^{-12}$	Atkinson et al. (2006)
BR38	OH + CHBr <sub>3</sub> → CBr <sub>3</sub> + H <sub>2</sub> O	$1.35 \times 10^{-12} e^{-600/T}$	Parrella et al. (2012)
BR39	OH + CH <sub>3</sub> Br → CH <sub>2</sub> Br + H <sub>2</sub> O	$2.35 \times 10^{-12} e^{-1,300/T}$	Sander et al. (2011)
BR40	OH + CH <sub>2</sub> Br <sub>2</sub> → CHBr <sub>2</sub> + H <sub>2</sub> O	$1.5 \times 10^{-12} e^{-775/T}$	Atkinson et al. (2008)
BR41	BrO + CH <sub>3</sub> O <sub>2</sub> → CH <sub>3</sub> O + BrOO	$1.4 \times 10^{-12}$	Atkinson et al. (2008)
BR42	BrO + CH <sub>3</sub> O <sub>2</sub> → HOBr + CH <sub>2</sub> O <sub>2</sub>	$4.3 \times 10^{-12}$	Atkinson et al. (2008)

**Acknowledgments**

This work was sponsored by the New York State Energy Research and Development Authority (NYSERDA) and the National Science Foundation of China grant 41475115. We thank R. Volkamer of University of Colorado for their BrO vertical profile measurement data. We are grateful to C. Hogrefe of US EPA for providing the 2010 WRF simulations. This work used XSEDE, which is supported by National Science Foundation grant ACI-1548562. We are grateful to the two anonymous reviewers for their thoughtful, detailed, constructive comments, which helped to improve the clarity of the paper. The observational ambient Hg data were downloaded from <http://nadp.sws.uiuc.edu/amn/data.aspx> (AMNet website) and <http://www.eos.unh.edu/observatories/data.shtml> (University of New Hampshire, 2016). Observational Hg wet deposition data were downloaded from <http://nadp.sws.uiuc.edu/data/MDN/> (MDN website). Hg dry deposition data used for comparison were derived from Zhang et al. (2012a, 2012b, 2016a), Yu et al. (2013), Risch et al. (2017), and Wang (2012).

**References**

Amos, H. M., Jacob, D. J., Holmes, C. D., Fisher, J. A., Wang, Q., Yantosca, R. M., et al. (2012). Gas-particle partitioning of atmospheric Hg(II) and its effect on global mercury deposition. *Atmospheric Chemistry and Physics*, 12(1), 591–603.

Ariya, P. A., Khalizov, A., & Gidas, A. (2002). Reactions of gaseous mercury with atomic and molecular halogens: Kinetics, product studies, and atmospheric implications. *Journal of Physical Chemistry A*, 106(32), 7310–7320.

Atkinson, R., Baulch, D. L., Cox, R. A., Crowley, J. N., Hampson, R. F., Hynes, R. G., et al. (2006). Evaluated kinetic and photochemical data for atmospheric chemistry: Volume II—Gas phase reactions of organic species. *Atmospheric Chemistry and Physics*, 6(11), 3625–4055. <https://doi.org/10.5194/acp-6-3625-2006>

Atkinson, R., Baulch, D. L., Cox, R. A., Crowley, J. N., Hampson, R. F., Hynes, R. G., et al. (2007). Evaluated kinetic and photochemical data for atmospheric chemistry: Volume III—Gas phase reactions of inorganic halogens. *Atmospheric Chemistry and Physics*, 7(4), 981–1191. <https://doi.org/10.5194/acp-7-981-2007>

- Atkinson, R., Baulch, D. L., Cox, R. A., Crowley, J. N., Hampson, R. F., Hynes, R. G., et al. (2008). Evaluated kinetic and photochemical data for atmospheric chemistry: Volume IV—Gas phase reactions of organic halogen species. *Atmospheric Chemistry and Physics*, 8(15), 4141–4496. <https://doi.org/10.5194/acp-8-4141-2008>
- Baker, K. R., & Bash, J. O. (2012). Regional scale photochemical model evaluation of total mercury wet deposition and speciated ambient mercury. *Atmospheric Environment*, 49, 151–162.
- Balabanov, N. B., Shepler, B. C., & Peterson, K. A. (2005). Accurate global potential energy surface and reaction dynamics for the ground state of HgBr<sub>2</sub>. *Journal of Physical Chemistry A*, 109(39), 8765–8773.
- Bash, J. O. (2010). Description and initial simulation of a dynamic bidirectional air-surface exchange model for mercury in Community Multiscale Air Quality (CMAQ) model. *Journal of Geophysical Research*, 115, D06305. <https://doi.org/10.1029/2009JD012834>
- Bash, J. O., Carlton, A. G., & Hutzell, W. T., & Russell Bullock, O., Jr. (2014). Regional air quality model application of the aqueous-phase photo reduction of atmospheric oxidized mercury by dicarboxylic acids. *Atmosphere*, 5(1), 1–15.
- Bieser, J., De Simone, F., Gencarelli, C., Geyer, B., Hedgecock, I., Matthias, V., et al. (2014). A diagnostic evaluation of modeled mercury wet depositions in Europe using atmospheric speciated high-resolution observations. *Environmental Science and Pollution Research*, 21(16), 9995–10012.
- Brooks, S., Ren, X., Cohen, M., Luke, W. T., Kelley, P., Artz, R., et al. (2014). Airborne vertical profiling of mercury speciation near Tullahoma, TN, USA. *Atmosphere*, 5(3), 557–574. <https://doi.org/10.3390/atmos5030557>
- Bullock, O. R., Jr., Atkinson, D., Braverman, T., Civerolo, K., Dastoor, A., Davignon, D., et al. (2008). The North American Mercury Model Inter-comparison Study (NAMMIS): Study description and model-to-model comparisons. *Journal of Geophysical Research*, 113, D17310. <https://doi.org/10.1029/2008JD009803>
- Bullock, O. R., Jr., Atkinson, D., Braverman, T., Civerolo, K., Dastoor, A., Davignon, D., et al. (2009). An analysis of simulated wet deposition of mercury from the North American Mercury Model Intercomparison Study. *Journal of Geophysical Research*, 114, D08301. <https://doi.org/10.1029/2008JD011224>
- Bullock, O. R., Jr., & Brehme, K. A. (2002). Atmospheric mercury simulation using the CMAQ model: Formulation description and analysis of wet deposition results. *Atmospheric Environment*, 36(13), 2135–2146.
- Bushey, J. T., Nallana, A. G., Montesdeoca, M. R., & Driscoll, C. T. (2008). Mercury dynamics of a northern hardwood canopy. *Atmospheric Environment*, 42(29), 6905–6914.
- Byun, D. W., & J. K. S. Ching (Eds.). (1999). *Science algorithms of the EPA Models-3 Community Multiscale Air Quality (CMAQ) modeling system* (Rep. EPA-600/R-99/030). Washington, DC: EPA.
- Calvert, J. G., & Lindberg, S. E. (2005). Mechanisms of mercury removal by O<sub>3</sub> and OH in the atmosphere. *Atmospheric Environment*, 39(18), 3355–3367.
- Chang, J. C., & Hanna, S. R. (2004). Air quality model performance evaluation. *Meteorology and Atmospheric Physics*, 87(1–3), 167–196. <https://doi.org/10.1007/s00703-003-0070-7>
- Chen, Q., Schmidt, J. A., Shah, V., Jaeglé, L., Sherwen, T., & Alexander, B. (2017). Sulfate production by reactive bromine: Implications for the global sulfur and reactive bromine budgets. *Geophysical Research Letters*, 44, 7069–7078. <https://doi.org/10.1002/2017GL073812>
- Choi, H.-D., Sharac, T. J., & Holsen, T. M. (2008). Mercury deposition in the Adirondacks: A comparison between precipitation and through-fall. *Atmospheric Environment*, 42(8), 1818–1827.
- Coburn, S., Dix, B., Edgerton, E., Holmes, C. D., Kinnison, D., Liang, Q., et al. (2016). Mercury oxidation from bromine chemistry in the free troposphere over the southeastern US. *Atmospheric Chemistry & Physics*, 16, 3743–3760. <https://doi.org/10.5194/acp-16-3743-2016>
- Cole, A. S., Steffen, A., Eckley, C. S., Narayan, J., Pilote, M., Tordon, R., et al. (2014). A survey of mercury in air and precipitation across Canada: Patterns and trends. *Atmosphere*, 5(3), 635–668. <https://doi.org/10.3390/atmos5030635>
- Dibble, T. S., Zelig, M. J., & Mao, H. (2012). Thermodynamics of reactions of ClHg and BrHg radicals with atmospherically abundant free radicals. *Atmospheric Chemistry and Physics*, 12(21), 10271–10279.
- Donohoue, D. L., Bauer, D., & Hynes, A. J. (2005). Temperature and pressure dependent rate coefficients for the reaction of Hg with Cl and the reaction of Cl with Cl: A pulsed laser photolysis-pulsed laser induced fluorescence study. *Journal of Physical Chemistry A*, 109(34), 7732–7741.
- Donohoue, D. L., Bauer, D., Cossairt, B., & Hynes, A. J. (2006). Temperature and pressure dependent rate coefficients for the reaction of Hg with Br and the reaction of Br with Br: A pulsed laser photolysis-pulsed laser induced fluorescence study. *Journal of Physical Chemistry A*, 110(21), 6623–6632.
- Driscoll, C. T., Mason, R. P., Chan, H. M., Jacob, D. J., & Pirrone, N. (2013). Mercury as a global pollutant: Sources, pathways, and effects. *Environmental Science and Technology*, 47(10), 4967–4983.
- Fitzgerald, W. F., Engstrom, D. R., Mason, R. P., & Nater, E. A. (1998). The case for atmospheric mercury contamination in remote areas. *Environmental Science and Technology*, 32(1), 1–7.
- Gay, D. A., Schmeltz, D., Prestbo, E., Olson, M., Sharac, T., & Tordon, R. (2013). The Atmospheric Mercury Network: Measurement and initial examination of an ongoing atmospheric mercury record across North America. *Atmospheric Chemistry and Physics*, 13(22), 11339–11349.
- Gbor, P. K., Wen, D., Meng, F., Yang, F., & Sloan, J. J. (2007). Modeling of mercury emission, transport and deposition in North America. *Atmospheric Environment*, 41(6), 1135–1149.
- Gbor, P. K., Wen, D., Meng, F., Yang, F., Zhang, B., & Sloan, J. J. (2006). Improved model for mercury emission, transport and deposition. *Atmospheric Environment*, 40(5), 973–983.
- Gencarelli, C. N., De Simone, F., Hedgecock, I. M., Sprovieri, F., Yang, X., & Pirrone, N. (2015). European and Mediterranean mercury modeling: Local and long-range contributions to the deposition flux. *Atmospheric Environment*, 117, 162–168. <https://doi.org/10.1016/j.atmosenv.2015.07.015>
- Gómez Martín, J. C., Mahajan, A. S., Hay, T. D., Prados-Román, C., Ordóñez, C., MacDonald, S. M., et al. (2013). Iodine chemistry in the eastern Pacific marine boundary layer. *Journal of Geophysical Research: Atmospheres*, 118, 887–904. <https://doi.org/10.1002/jgrd.50132>
- Goodsite, M. E., Plane, J. M. C., & Skov, H. (2004). A theoretical study of the oxidation of Hg<sup>0</sup> to HgBr<sub>2</sub> in the troposphere. *Environmental Science & Technology*, 38(6), 1772–1776. <https://doi.org/10.1021/es034680s>
- Goodsite, M. E., Plane, J. M. C., & Skov, H. (2012). Erratum: A theoretical study of the oxidation of Hg<sup>0</sup> to HgBr<sub>2</sub> in the troposphere. *Environmental Science and Technology*, 38(6), 1772–1776. <https://doi.org/10.1021/es301201c>
- Grant, S. L., Kim, M., Lin, P., Crist, K. C., Ghosh, S., & Kotamarthi, V. R. (2014). A simulation study of atmospheric mercury and its deposition in the Great Lakes. *Atmospheric Environment*, 94, 164–172. <https://doi.org/10.1016/j.atmosenv.2014.05.033>
- Gratz, L. E., Ambrose, J. L., Jaffe, D. A., Shah, V., Jaeglé, L., Stutz, J., et al. (2015). Oxidation of mercury by bromine in the subtropical Pacific free troposphere. *Geophysical Research Letters*, 42, 10494–10502. <https://doi.org/10.1002/2015GL066645>
- Gustin, M. S., Amos, H. M., Huang, J., Miller, M. B., & Heidecorn, K. (2015). Measuring and modeling mercury in the atmosphere: A critical review. *Atmospheric Chemistry and Physics*, 15(10), 5697–5713. <https://doi.org/10.5194/acp-15-5697-2015>

- Gustin, M. S., Huang, J., Miller, M. B., Peterson, C., Jaffe, D. A., Ambrose, J., et al. (2013). Do we understand what the mercury speciation instruments are actually measuring? Results of RAMIX. *Environmental Science and Technology*, *47*(13), 7295–7306.
- Hall, B. (1995). The gas phase oxidation of elemental mercury by ozone. *Water, Air, and Soil Pollution*, *80*(1–4), 301–315.
- Hanna, S. R. (1988). Air quality model evaluation and uncertainty. *JAPCA*, *38*(4), 406–412. <https://doi.org/10.1080/08940630.1988.10466390>
- Hanna, S. R., Chang, J. C., & Strimaitis, D. G. (1993). Hazardous gas model evaluation with field observations. *Atmospheric Environment. Part A. General Topics*, *27*(15), 2265–2285. [https://doi.org/10.1016/0960-1686\(93\)90397-H](https://doi.org/10.1016/0960-1686(93)90397-H)
- Hanna, S. R., Strimaitis, D. G., & Chang, J. C. (1991a). *Hazard response modeling uncertainty (a quantitative method), vol. 1: User's guide for software for evaluating hazardous gas dispersion models*. Washington, DC: API.
- Hanna, S. R., Strimaitis, D. G., & Chang, J. C. (1991b). *Hazard response modeling uncertainty (a quantitative method), vol. II: Evaluation of commonly-used hazardous gas dispersion models*. Washington, DC: API.
- Hanna, S. R., Strimaitis, D. G., & Chang, J. C. (1991c). *Hazard response modeling uncertainty (a quantitative method), vol. III: Components of uncertainty in hazardous gas dispersion models*. Washington, DC: API.
- Holloway, T., Voigt, C., Morton, J., Spak, S. N., Rutter, A. P., & Schauer, J. J. (2012). An assessment of atmospheric mercury in the Community Multiscale Air Quality (CMAQ) model at an urban site and a rural site in the Great Lakes Region of North America. *Atmospheric Chemistry and Physics*, *12*(15), 7117–7133.
- Holmes, C. D., Jacob, D. J., Corbitt, E. S., Mao, J., Yang, X., Talbot, R., et al. (2010). Global atmospheric model for mercury including oxidation by bromine atoms. *Atmospheric Chemistry and Physics*, *10*(24), 12037–12057.
- Holmes, C. D., Jacob, D. J., Mason, R. P., & Jaffe, D. A. (2009). Sources and deposition of reactive gaseous mercury in the marine atmosphere. *Atmospheric Environment*, *43*(14), 2278–2285.
- Holmes, C. D., Jacob, D. J., & Yang, X. (2006). Global lifetime of elemental mercury against oxidation by atomic bromine in the free troposphere. *Geophysical Research Letters*, *33*, L20808. <https://doi.org/10.1029/2006GL027176>
- Holmes, C. D., Krishnamurthy, N. P., Caffrey, J. M., Landing, W. M., Edgerton, E. S., Knapp, K. R., et al. (2016). Thunderstorms increase mercury wet deposition. *Environmental Science and Technology*, *50*(17), 9343–9350. <https://doi.org/10.1021/acs.est.6b02586>
- Horowitz, H. M., Jacob, D. J., Zhang, Y., Dibble, T. S., Slemr, F., Amos, H. M., et al. (2017). A new mechanism for atmospheric mercury redox chemistry: Implications for the global mercury budget. *Atmospheric Chemistry and Physics*, *17*(10), 6353–6371. <https://doi.org/10.5194/acp-17-6353-2017>
- Houyoux, M. R., Vukovich, J. M., Coats, C. J., Wheeler, N. J. M., & Kasibhatla, P. S. (2000). Emission inventory development and processing for the Seasonal Model for Regional Air Quality (SMRAQ) project. *Journal of Geophysical Research*, *105*(D7), 9079–9090. <https://doi.org/10.1029/1999JD900975>
- Huang, J., & Gustin, M. S. (2015). Uncertainties of gaseous oxidized mercury measurements using KCl-coated denuders, cation-exchange membranes, and nylon membranes: Humidity influences. *Environmental Science & Technology*, *49*(10), 6102–6108. <https://doi.org/10.1021/acs.est.5b00098>
- Hynes, A. J., Donohoue, D. L., Goodsite, M. E., & Hedgecock, I. M. (2009). Our current understanding of major chemical and physical processes affecting mercury dynamics in the atmosphere and at the air-water/terrestrial interfaces. *Mercury Fate and Transport in the Global Atmosphere: Emissions, Measurements and Models*, 427–457.
- Jaffe, D. A., Lyman, S., Amos, H. M., Gustin, M. S., Huang, J., Selin, N. E., et al. (2014). Progress on understanding atmospheric mercury hampered by uncertain measurements. *Environmental Science & Technology*, *48*(13), 7204–7206. <https://doi.org/10.1021/es5026432>
- Jiao, Y., & Dibble, T. S. (2017). First kinetic study of the atmospherically important reactions  $\text{BrHg} + \text{NO}_2$  and  $\text{BrHg} + \text{HO}$ . *Physical Chemistry Chemical Physics*, *19*(3), 1826–1838. <https://doi.org/10.1039/C6CP06276H>
- Jones, C. P., Lyman, S. N., Jaffe, D. A., Allen, T., & O'Neil, T. L. (2016). Detection and quantification of gas-phase oxidized mercury compounds by GC/MS. *Atmospheric Measurement Techniques*, *9*(5), 2195–2205. <https://doi.org/10.5194/amt-9-2195-2016>
- Kos, G., Ryzhkov, A., Dastoor, A., Narayan, J., Steffen, A., Ariya, P. A., et al. (2013). Evaluation of discrepancy between measured and modelled oxidized mercury species. *Atmospheric Chemistry and Physics*, *13*(9), 4839–4863. <https://doi.org/10.5194/acp-13-4839-2013>
- Li, Z., Jeong, G.-R., & Person, E. (2002). Kinetics of reactions of OBrO with NO, O<sub>3</sub>, OClO, and ClO at 240–350 K. *International Journal of Chemical Kinetics*, *34*(7), 430–437. <https://doi.org/10.1002/kin.10069>
- Lin, C.-J., Pan, L., Streets, D. G., Shetty, S. K., Jang, C., Feng, X., et al. (2010). Estimating mercury emission outflow from East Asia using CMAQ-Hg. *Atmospheric Chemistry and Physics*, *10*(4), 1853–1864.
- Lin, C.-J., Pongprueksa P., Bullock, O. R., Jr., Lindberg, S. E., Pehkonen, S. O., Jang, C., et al. (2007). Scientific uncertainties in atmospheric mercury models II: Sensitivity analysis in the CONUS domain. *Atmospheric Environment*, *41*(31), 6544–6560.
- Lin, C.-J., Pongprueksa, P., Lindberg, S. E., Pehkonen, S. O., Byun, D., & Jang, C. (2006). Scientific uncertainties in atmospheric mercury models I: Model science evaluation. *Atmospheric Environment*, *40*(16), 2911–2928.
- Lin, C.-J., Shetty, S. K., Pan, L., Pongprueksa, P., Jang, C., & Chu, H.-W. (2012). Source attribution for mercury deposition in the contiguous United States: Regional difference and seasonal variation. *Journal of the Air and Waste Management Association*, *62*(1), 52–63.
- Lin, X., & Tao, Y. (2003). A numerical modelling study on regional mercury budget for eastern North America. *Atmospheric Chemistry and Physics*, *3*(3), 535–548.
- Lu, D., Cizdziel, J. V., Jiang, Y., White, L., & Reddy, R. S. (2014). Numerical simulation of atmospheric mercury in mid-south USA. *Air Quality, Atmosphere and Health*, *7*(4), 525–540. <https://doi.org/10.1007/s11869-014-0256-9>
- Lyman, S. N., & Jaffe, D. A. (2012). Formation and fate of oxidized mercury in the upper troposphere and lower stratosphere. *Nature Geoscience*, *5*(2), 114–117. <https://doi.org/10.1038/ngeo1353>
- Lyman, S. N., Jaffe, D. A., & Gustin, M. S. (2010). Release of mercury halides from KCl denuders in the presence of ozone. *Atmospheric Chemistry and Physics*, *10*(17), 8197–8204. <https://doi.org/10.5194/acp-10-8197-2010>
- Mao, H., Cheng, I., & Zhang, L. (2016). Current understanding of the driving mechanisms for spatiotemporal variations of atmospheric speciated mercury: A review. *Atmospheric Chemistry and Physics*, *16*(20), 12897–12924. <https://doi.org/10.5194/acp-16-12897-2016>
- Mao, H., & Talbot, R. (2012). Speciated mercury at marine, coastal, and inland sites in New England—Part 1: Temporal variability. *Atmospheric Chemistry and Physics*, *12*(11), 5099–5112.
- Mao, H., Talbot, R. W., Sive, B. C., Kim, S. Y., Blake, D. R., & Weinheimer, A. J. (2010). Arctic mercury depletion and its quantitative link with halogens. *Journal of Atmospheric Chemistry*, *65*(2–3), 145–170.
- Mason, R. P., Kim, E.-H., Cornwell, J., & Heyes, D. (2006). An examination of the factors influencing the flux of mercury, methylmercury and other constituents from estuarine sediment. *Marine Chemistry*, *102*(1–2), 96–110.
- McClure, C. D., Jaffe, D. A., & Edgerton, E. S. (2014). Evaluation of the KCl denuder method for gaseous oxidized mercury using HgBr<sub>2</sub> at an in-service AMNet site. *Environmental Science and Technology*, *48*(19), 11437–11444. <https://doi.org/10.1021/es502545k>

- Mellouki, A., Poulet, G., Le Bras, G., Singer, R., Burrows, J. P., & Moortgat, G. K. (1989). Discharge flow kinetic study of the reactions of nitrate radical with bromine, bromine monoxide, hydrogen bromide, and hydrogen chloride. *The Journal of Physical Chemistry*, 93(24), 8017–8021. <https://doi.org/10.1021/j100361a012>
- Michalakes, J., Dudhia, J., Gill, D., Henderson, T., Klemp, J., Skamarock, W., et al. (2004). *The Weather Research and Forecast model: Software architecture and performance*. Paper presented at the Proceedings of the 11th ECMWF Workshop on the use of high performance computing in meteorology, Reading, UK, October 25–29, 2004.
- Miller, C. L., Mason, R. P., Gilmour, C. C., & Heyes, A. (2007). Influence of dissolved organic matter on the complexation of mercury under sulfidic conditions. *Environmental Toxicology and Chemistry*, 26(4), 624–633.
- Myers, T., R. D., Atkinson, Bullock, O. R., Jr., & Bash, J. O. (2013). Investigation of effects of varying model inputs on mercury deposition estimates in the Southwest US. *Atmospheric Chemistry and Physics*, 13(2), 997–1009.
- Obrist, D., Tas, E., Peleg, M., Matveev, V., Faïn, X., Asaf, D., et al. (2011). Bromine-induced oxidation of mercury in the mid-latitude atmosphere. *Nature Geoscience*, 4(1), 22–26. <https://doi.org/10.1038/ngeo1018>
- Orlando, J. J., & Tyndall, G. S. (1996). Rate coefficients for the thermal decomposition of BrONO<sub>2</sub> and the heat of formation of BrONO<sub>2</sub>. *Journal of Physical Chemistry*, 100(50), 19398–19405.
- Pal, B., & Ariya, P. A. (2004). Gas-phase HO-initiated reactions of elemental mercury: Kinetics, product studies, and atmospheric implications. *Environmental Science and Technology*, 38(21), 5555–5566.
- Parrella, J. P., Jacob, D. J., Liang, Q., Zhang, Y., Mickley, L. J., Miller, B., et al. (2012). Tropospheric bromine chemistry: Implications for present and pre-industrial ozone and mercury. *Atmospheric Chemistry and Physics*, 12(15), 6723–6740.
- Pleim, J. E., & Byun, D. W. (2004). Application of a new land-surface, dry deposition, and PBL model in the Models-3 Community Multi-scale Air Quality (CMAQ) model system. In S.-E. Gryning & K. L. Schere (Eds.), *Air pollution modeling and its application XIV* (pp. 297–305). New York, NY: Springer.
- Pluel, K., & Munthe, J. (1995). Modelling the atmospheric mercury cycle-chemistry in fog droplets. *Atmospheric Environment*, 29(12), 1441–1457. [https://doi.org/10.1016/1352-2310\(94\)00323-D](https://doi.org/10.1016/1352-2310(94)00323-D)
- Pongprueksa, P., Lin, C. J., Lindberg, S. E., Jang, C., Braverman, T., Bullock, O. R., Jr., et al. (2008). Scientific uncertainties in atmospheric mercury models III: Boundary and initial conditions, model grid resolution, and Hg(II) reduction mechanism. *Atmospheric Environment*, 42(8), 1828–1845.
- Raofie, F., & Ariya, P. A. (2003). Kinetics and products study of the reaction of BrO radicals with gaseous mercury. *Journal De Physique. IV: JP*, 107, 1119–1121.
- Raofie, F., & Ariya, P. A. (2004). Product study of the gas-phase BrO-initiated oxidation of Hg<sup>0</sup>: Evidence for stable Hg<sup>1+</sup> compounds. *Environmental Science and Technology*, 38(16), 4319–4326.
- Risch, M. R., DeWild, J. F., Gay, D. A., Zhang, L., Boyer, E. W., & Krabbenhoft, D. P. (2017). Atmospheric mercury deposition to forests in the eastern USA. *Environmental Pollution*, 228, 8–18. <https://doi.org/10.1016/j.envpol.2017.05.004>
- Risch, M. R., DeWild, J. F., Krabbenhoft, D. P., Kolka, R. K., & Zhang, L. (2012). Litterfall mercury dry deposition in the eastern USA. *Environmental Pollution*, 161, 284–290. <https://doi.org/10.1016/j.envpol.2011.06.005>
- Rolfhus, K. R., Sakamoto, H. E., Cleckner, L. B., Stoor, R. W., Babiartz, C. L., Back, R. C., et al. (2003). Distribution and fluxes of total and methylmercury in Lake Superior. *Environmental Science and Technology*, 37(5), 865–872.
- Ryaboshapko, A., Bullock, O. R., Jr., Christensen, J., Cohen, M., Dastoor, A., Ilyin, I., et al. (2007). Intercomparison study of atmospheric mercury models: 2. Modelling results vs. long-term observations and comparison of country deposition budgets. *Science of the Total Environment*, 377(2–3), 319–333.
- Sander, S. P., Abbatt, J., Barker, J., Burkholder, J. B., Friedl, R. R., Golden, D. M., et al. (2011). *Chemical kinetics and photochemical data for use in atmospheric studies* (Evaluation No. 17). Pasadena, CA: Jet Propulsion Laboratory.
- Sander, S. P., Finlayson-Pitts, B., Friedl, R. R., Golden, D. M., Huie, R., Keller-Rudek, H., et al. (2006). *Chemical kinetics and photochemical data for use in atmospheric studies* (Evaluation No. 15). Pasadena, CA: Jet Propulsion Laboratory.
- Sander, S. P., & Watson, R. T. (1981). Kinetics and mechanism of the disproportionation of bromine oxide (BrO) radicals. *Journal of Physical Chemistry*, 85(26), 4000–4007.
- Sarwar, G., Luecken, D., Yarwood, G., Whitten, G. Z., & Carter, W. P. L. (2008). Impact of an updated carbon bond mechanism on predictions from the CMAQ modeling system: Preliminary assessment. *Journal of Applied Meteorology and Climatology*, 47(1), 3–14. <https://doi.org/10.1175/2007JAMC1393.1>
- Schmidt, J. A., Jacob, D. J., Horowitz, H. M., Hu, L., Sherwen, T., Evans, M. J., et al. (2016). Modeling the observed tropospheric BrO background: Importance of multiphase chemistry and implications for ozone, OH, and mercury. *Journal of Geophysical Research: Atmospheres*, 121(19), 2015JD024229. <https://doi.org/10.1002/2015JD024229>
- Seigneur, C., Vijayaraghavan, K., Lohman, K., Karamchandani, P., & Scott, C. (2004). Global source attribution for mercury deposition in the United States. *Environmental Science and Technology*, 38(2), 555–569.
- Selin, N. E., Javob, D. J., Park, R. J., Yantosca, R., Strode, M., Jaeglé, S. L., et al. (2007). Chemical cycling and deposition of atmospheric mercury: Global constraints from observations. *Journal of Geophysical Research*, 112, D02308. <https://doi.org/10.1029/2006JD007450>
- Shah, V., Jaeglé, L., Gratz, L. E., Ambrose, J. L., Jaffe, D. A., Selin, N. E., et al. (2016). Origin of oxidized mercury in the summertime free troposphere over the southeastern US. *Atmospheric Chemistry and Physics*, 16(3), 1511–1530. <https://doi.org/10.5194/acp-16-1511-2016>
- Si, L., & Ariya, P. A. (2008). Reduction of oxidized mercury species by dicarboxylic acids (C<sub>2</sub>–C<sub>4</sub>): Kinetic and product studies. *Environmental Science and Technology*, 42(14), 5150–5155.
- Sigler, J. M., Mao, H., & Talbot, R. (2009). Gaseous elemental and reactive mercury in Southern New Hampshire. *Atmospheric Chemistry and Physics*, 9(6), 1929–1942. <https://doi.org/10.5194/acp-9-1929-2009>
- Sillman, S., Marsik, F. J., Al-Wali, K. I., Keeler, G. J., & Landis, M. S. (2007). Reactive mercury in the troposphere: Model formation and results for Florida, the northeastern United States, and the Atlantic Ocean. *Journal of Geophysical Research*, 112, D23305. <https://doi.org/10.1029/2006JD008227>
- Skamarock, W. C., Klemp, J. B., Dudhia, J., Gill, D. O., Barker, D. M., Duda, M. G., et al. (2008). *A description of the advanced research WRF version 3* (NCAR Tech. Note NCAR/TN-475+STR). Boulder, CO: NCAR. <https://doi.org/10.5065/D68S4MVH>
- Smith-Downey, N. V., Sunderland, E. M., & Jacob, D. J. (2010). Anthropogenic impacts on global storage and emissions of mercury from terrestrial soils: Insights from a new global model. *Journal of Geophysical Research*, 115, G03008. <https://doi.org/10.1029/2009JG001124>
- Soerensen, A. L., Mason, R. P., Balcom, P. H., & Sunderland, E. M. (2013). Drivers of surface ocean mercury concentrations and air-sea exchange in the West Atlantic Ocean. *Environmental Science and Technology*, 47, 7757–7765. <https://doi.org/10.1021/es401354q>
- Sommar, J., Gärdfeldt, K., Strömberg, D., & Feng, X. (2001). A kinetic study of the gas-phase reaction between the hydroxyl radical and atomic mercury. *Atmospheric Environment*, 35(17), 3049–3054.

- Spicer, C. W., Satola, J., Abby, A. A., Plastring, R. A., & Cowen, K. A. (2002). *Kinetics of gas-phase elemental mercury reaction with halogen species, ozone, and nitrate radical under atmospheric conditions* (Final Report). Florida Department of Environmental Protection, FL.
- Subir, M., Ariya, P. A., & Dastoor, A. P. (2011). A review of uncertainties in atmospheric modeling of mercury chemistry I. Uncertainties in existing kinetic parameters—Fundamental limitations and the importance of heterogeneous chemistry. *Atmospheric Environment*, 45(32), 5664–5676.
- Sunderland, E. M., Cohen, M. D., Selin, N. E., & Chmura, G. L. (2008). Reconciling models and measurements to assess trends in atmospheric mercury deposition. *Environmental Pollution*, 156(2), 526–535.
- Tanaka, P. L., Allen, D. T., McDonald-Buller, E. C., Chang, S., Kimura, Y., Mullins, C. B., et al. (2003). Development of a chlorine mechanism for use in the carbon bond IV chemistry model. *Journal of Geophysical Research*, 108(D4), 4145. <https://doi.org/10.1029/2002JD002432>
- Tokos, J. J. S., Hall, B., Calhoun, J. A., & Prestbo, E. M. (1998). Homogeneous gas-phase reaction of Hg<sup>0</sup> with H<sub>2</sub>O<sub>2</sub>, O<sub>3</sub>, CH<sub>3</sub>I, and (CH<sub>3</sub>)<sub>2</sub>S: Implications for atmospheric Hg cycling. *Atmospheric Environment*, 32(5), 823–827.
- Tossell, J. A. (2003). Calculation of the energetics for oxidation of gas-phase elemental Hg by Br and BrO. *Journal of Physical Chemistry A*, 107(39), 7804–7808.
- Towns, J., Cockerill, T., Dahan, M., Foster, I., Gaither, K., Grimshaw, A., et al. (2014). XSEDE: Accelerating scientific discovery. *Computing in Science & Engineering*, 16(5), 62–74.
- Vermette, S. J., Peden, M. E., Willoughby, T. C., Lindberg, S. E., & Weiss, A. D. (1995). Methodology for the sampling of metals in precipitation: Results of the National Atmospheric Deposition Program (NADP) pilot network. *Atmospheric Environment*, 29(11), 1221–1229. [https://doi.org/10.1016/1352-2310\(94\)00207-2](https://doi.org/10.1016/1352-2310(94)00207-2)
- Vijayaraghavan, K., Seigneur, C., Karamchandani, P., & Chen, S.-Y. (2007). Development and application of a multipollutant model for atmospheric mercury deposition. *Journal of Applied Meteorology and Climatology*, 46(9), 1341–1353. <https://doi.org/10.1175/JAM2536.1>
- Volkamer, R., Baidar, S., Campos, T. L., Coburn, S., DiGangi, J. P., Dix, B., et al. (2015). Aircraft measurements of BrO, IO, glyoxal, NO<sub>2</sub>, H<sub>2</sub>O, O<sub>2</sub>-O<sub>2</sub> and aerosol extinction profiles in the tropics: Comparison with aircraft-/ship-based in situ and lidar measurements. *Atmospheric Measurement Techniques*, 8(5), 2121–2148. <https://doi.org/10.5194/amt-8-2121-2015>
- Wang, F., Saiz-Lopez, A., Mahajan, A. S., Martín, J. C. G., Armstrong, D., Lemes, M., et al. (2014). Enhanced production of oxidised mercury over the tropical Pacific Ocean: A key missing oxidation pathway. *Atmospheric Chemistry and Physics*, 14(3), 1323–1335.
- Wang, S., Schmidt, J. A., Baidar, S., Coburn, S., Dix, B., Koenig, T. K., et al. (2015). Active and widespread halogen chemistry in the tropical and subtropical free troposphere. *Proceedings of the National Academy of Sciences of the United States of America*, 112(30), 9281–9286. <https://doi.org/10.1073/pnas.1505142112>
- Wang, X. (2012). *Seasonal variations in the inputs and fate of mercury in a Northern hardwood forest* (MS thesis). Syracuse, NY: Syracuse University.
- Weiss-Penzias, P. S., Gay, D. A., Brigham, M. E., Parsons, M. T., Gustin, M. S., & ter Schure, A. (2016). Trends in mercury wet deposition and mercury air concentrations across the U.S. and Canada. *Science of the Total Environment*, 568, 546–556. <https://doi.org/10.1016/j.scitotenv.2016.01.061>
- Wen, D., Lin, J. C., Meng, F., Gbor, P. K., He, Z., & Sloan, J. J. (2011). Quantitative assessment of upstream source influences on total gaseous mercury observations in Ontario, Canada. *Atmospheric Chemistry and Physics*, 11(4), 1405–1415.
- Whitten, G. Z., Heo, G., Kimura, Y., McDonald-Buller, E., Allen, D. T., Carter, W. P. L., et al. (2010). A new condensed toluene mechanism for Carbon Bond: CB05-TU. *Atmospheric Environment*, 44(40), 5346–5355. <https://doi.org/10.1016/j.atmosenv.2009.12.029>
- Wright, L. P., Zhang, L., & Marsik, F. J. (2016). Overview of mercury dry deposition, litterfall, and throughfall studies. *Atmospheric Chemistry and Physics*, 16(21), 13399–13416. <https://doi.org/10.5194/acp-16-13399-2016>
- Yarwood, G., Rao, S., Yocke, M., & Whitten, G. (2005). *Updates to the carbon bond chemical mechanism: CB05* (Rep. RT-0400675). Washington, DC: US EPA. Retrieved from [http://www.camx.com/files/cb05\\_final\\_report\\_120805.aspx](http://www.camx.com/files/cb05_final_report_120805.aspx)
- Ye, Z., Mao, H., Lin, C.-J., & Kim, S. Y. (2016). Investigation of processes controlling summertime gaseous elemental mercury oxidation at midlatitudinal marine, coastal, and inland sites. *Atmospheric Chemistry and Physics*, 16(13), 8461–8478. <https://doi.org/10.5194/acp-16-8461-2016>
- Yu, X., Driscoll, C. T., Huang, J., Holsen, T. M., & Blackwell, B. D. (2013). Modeling and mapping of atmospheric mercury deposition in Adirondack Park, New York. *PLoS ONE*, 8(3), e59322.
- Zhang, L., Blanchard, P., Gay, D. A., Prestbo, E. M., Risch, M. R., Johnson, D., et al. (2012b). Estimation of speciated and total mercury dry deposition at monitoring locations in eastern and central North America. *Atmospheric Chemistry and Physics*, 12(9), 4327–4340.
- Zhang, L., Blanchard, P., Johnson, D., Dastoor, A., Ryzhkov, A., Lin, C. J., et al. (2012a). Assessment of modeled mercury dry deposition over the Great Lakes region. *Environmental Pollution*, 161, 272–283. <https://doi.org/10.1016/j.envpol.2011.06.003>
- Zhang, L., Lyman, S., Mao, H., Lin, C.-J., Gay, D. A., Wang, S., et al. (2017). A synthesis of research needs for improving the understanding of atmospheric mercury cycling. *Atmospheric Chemistry and Physics Discussion*, 17, 9133–9144. <https://doi.org/10.5194/acp-17-9133-2017>
- Zhang, L., Wu, Z., Cheng, I., Wright, L. P., Olson, M. L., Gay, D. A., et al. (2016a). The estimated six-year mercury dry deposition across North America. *Environmental Science and Technology*, 50(23), 12864–12873. <https://doi.org/10.1021/acs.est.6b04276>
- Zhang, Y., & Jaeglé, L. (2013). Decreases in mercury wet deposition over the United States during 2004–2010: Roles of domestic and global background emission reductions. *Atmosphere*, 4(2), 113–131. <https://doi.org/10.3390/atmos4020113>
- Zhang, Y., Jaeglé, L., van Donkelaar, A., Martin, R. V., Holmes, C. D., Amos, H. M., et al. (2012c). Nested-grid simulation of mercury over North America. *Atmospheric Chemistry and Physics*, 12(14), 6095–6111. <https://doi.org/10.5194/acp-12-6095-2012>
- Zhang, Y., Jacob, D. J., Horowitz, H. M., Chen, L., Amos, H. M., Krabbenhoft, D. P., et al. (2016b). Observed decrease in atmospheric mercury explained by global decline in anthropogenic emissions. *Proceedings of the National Academy of Sciences of the United States of America*, 113(3), 526–531. <https://doi.org/10.1073/pnas.1516312113>
- Zhu, J., Wang, T., Bieser, J., & Matthias, V. (2015). Source attribution and process analysis for atmospheric mercury in eastern China simulated by CMAQ-Hg. *Atmospheric Chemistry and Physics*, 15(15), 8767–8779. <https://doi.org/10.5194/acp-15-8767-2015>